Method-of-double-moments for cryo-electron microscopy

Joe Kileel, Oscar Mickelin, Amit Singer, Sheng Xu

October 14, 2025

Abstract

Cryo-electron microscopy is an advanced and increasingly popular imaging technique for reconstructing three-dimensional structures from noisy and randomly oriented tomographic projection images. We introduce an algorithm, termed the method-of-double-moments, to reconstruct the structure using two instances of the second moment of the projection images, which are generated from two different distributions of random orientations (e.g., arising from different experimental conditions), where one distribution is uniform and the other is non-uniform and unknown. We prove that these moments generically uniquely identify the structure, up to a global rotation and reflection. Furthermore, we devise a convex relaxation-based algorithm which numerically recovers bandlimited structures from only their second moments.

1 Introduction

Cryo-electron microscopy (cryo-EM) is an increasingly popular technique for single-particle reconstruction [19, 25, 3, 13]. It aims to reconstruct three-dimensional structures from noisy and randomly oriented tomographic projection images, with applications in structural biology, medicine, and drug discovery [31, 42, 16, 35, 44]. This paper introduces a new method to perform the 3-D reconstruction, using low-order statistics (namely two instances of the second-order moments) of the projection images. Crucially, we prove that these statistics uniquely identify the structure and devise a numerically efficient reconstruction scheme.

This approach to the problem provably has sample complexity $\omega(\sigma^4)$, where σ^2 is the signal-to-noise ratio. Our results improve on previous work using the method-of-moments which either assume access to higher-order moments (which implies a significantly higher sample complexity of at least $\omega(\sigma^6)$), make generative assumptions on the structure, only identify the structure up to a finite list of candidates instead of uniquely, or do not provably guarantee uniqueness. Additionally, previous numerical methods are prone to stagnation or convergence to spurious local minima. See Section 1.2 for a more detailed discussion of related works.

The remainder of this paper is organized as follows. Section **??** introduces notation. Section 1.1 introduces the image formation model considered in cryo-EM and Section 1.2

discusses related work. Section 2 details the assumptions and conventions used in the paper, precisely states the main problem, and presents the main result. Section 4 presents the algorithm for solving the problem. Section 5 proves that the algorithm has a unique solution. Section **??** provides empirical numerical evidence that the algorithm converges to this solution, for any initialization of the problem variables.

1.1 Image formation model

Denoting the electrostatic potential of a 3-D structure by $\Phi : \mathbb{R}^3 \to \mathbb{R}$ and a sample random rotation by $R \in \mathsf{SO}(3)$, we denote the action of R on Φ by $R \cdot \Phi : \mathbb{R}^3 \to \mathbb{R}$, and define this rotated function by

$$(R^\mathsf{T} \cdot \Phi)(x, y, z) := \Phi\left(R(x, y, z)\right). \tag{1.1}$$

We model the formation of the tomographic projection image $I_R(x, y)$ corresponding to the rotation R by

$$I_R(x, y) = \int_{-\infty}^{\infty} (R^\mathsf{T} \cdot \Phi)(x, y, z)dz + \varepsilon(x, y), \tag{1.2}$$

where ε is a noise term assumed to be white Gaussian noise with variance $\sigma^2 I$ and independent of the signal term, whose statistics can be estimated from the projection image, and the rotation R follows some unknown probability distribution ρ. Experiments produce projection images $I_{R_1}, \ldots, I_{R_N}$, where the rotations R_i for $i = 1, \ldots, N$ are unknown samples from the distribution ρ. Due to high levels of noise present in the projection images, a typical experiment requires tens of thousands of projection images, if not more, to obtain reasonable reconstruction resolution [3, 44].

A slightly more involved model also includes the effect of aberrations in the image formation model, through convolution with the so called point spread function $h_i(x, y)$, whose Fourier transform is known as the contrast transfer function [39]. Typically, each h_i is a radial and highly oscillatory function with frequent zero crossings. The image formation is then modelled as

$$I_{R_i}(x, y) = h_i(x, y) * \int_{-\infty}^{\infty} (R_i^\mathsf{T} \cdot \Phi)(x, y, z)dz + \varepsilon(x, y).$$

In the proposed algorithm, the projection images I_{R_i} are used only to estimate the second-order moment. When doing so, the effect of the point spread function can be corrected, provided the functions h_i for $i = 1, \ldots, N$ have sufficiently non-overlapping zero-crossings [36, 28]. We therefore omit point spread functions in the following, by assuming that this correction has been performed.

1.2 Existing methods

1.2.1 3-D Iterative refinement

Popular state-of-the-art methods typically employ expectation-maximization algorithms in a procedure known as 3-D iterative refinement [37, 32]. However, no global convergence guarantees are known for this method [38, 39]. This is problematic for certain downstream applications of cryo-EM reconstruction, such as drug design, where reliability is critical. In order to avoid convergence to local minima, successful reconstruction therefore requires initialization sufficiently close to the ground truth and an unsuitable choice could lead to bias in the reconstruction [38, 39]. The techniques are computationally expensive and require accessing the entire dataset $I_{R_1}, \ldots, I_{R_N}$ during each iteration of the refinement.

1.2.2 Method-of-moments

An alternative approach uses the method-of-moments, wherein experimental data is used to estimate empirical moments of the *Fourier transforms* of the projection images, to increasing orders. The kth-order empirical moment $\widetilde{m}_k : \mathbb{R}^{2k} \to \mathbb{C}$ is given by[1]

$$\widetilde{m}_k\left(\mathbf{x}_1, \ldots, \mathbf{x}_k\right) := \frac{1}{N} \sum_{i=1}^{N} \widehat{I}_{R_i}(\mathbf{x}_1) \cdots \widehat{I}_{R_i}(\mathbf{x}_{k-1}) \overline{\widehat{I}_{R_i}(\mathbf{x}_k)} - B_k(\mathbf{x}_1, \ldots, \mathbf{x}_k, \sigma), \tag{1.3}$$

where $\mathbf{x}_j \in \mathbb{R}^2$ for $j = 1, \ldots, k$, and $B_k(\mathbf{x}_1, \ldots, \mathbf{x}_k, \sigma)$ denotes a debias term that depends on the noise variance of the projection images (which we assume has been estimated from the projection images). When we wish to emphasize the dependence of the moments on the molecular structure Φ and the rotational distribution ρ, we will also write $\widetilde{m}_k[\Phi, \rho]$, where the ρ-dependence influences the moments through the sampled projection images.

The method-of-moments attempts to reconstruct the molecular structure from the moments by matching the empirical moments to the population moments $m_k : \mathbb{R}^{2k} \to \mathbb{C}$

$$m_k(\mathbf{x}_1, \ldots, \mathbf{x}_k) := \int_{\mathsf{SO}(3)} \widehat{I}_R(\mathbf{x}_1) \cdots \widehat{I}_R(\mathbf{x}_{k-1}) \overline{\widehat{I}_R(\mathbf{x}_k)} \rho(R) \mathrm{d}R - B_k(\mathbf{x}_1, \ldots, \mathbf{x}_k, \sigma), \tag{1.4}$$

by e.g., solving $\min_{\Phi,\rho} \sum_{k=1}^{d} \lambda_k \|\widetilde{m}_k - m_k[\Phi, \rho]\|_2^2$, for some suitably chosen weights $\lambda_k \in \mathbb{R}_{\geq 0}$, where $k = 1, \ldots, d$.

One or two passes over the data suffice to estimate the moments in (1.3), after which the dataset does not need to be accessed [46, 8, 36, 28], resulting in lower computational complexity compared to iterative refinement for sufficiently large datasets. Another advantage of the method-of-moments compared to 3-D iterative refinement is in reconstructing small molecules (e.g., below 40 kDa), where state-of-the-art software implementations of 3-D iterative refinement encounter challenges [32, 30]. Identifying individual particle locations is however still possible for these molecules [43, figure 10 f–h], so it is possible to form the sample moments and the method-of-moments can therefore still be applied.

In the context of cryo-EM, the method-of-moments was originally introduced in 1980 [24] and it was observed numerically that the population moments of order $d = 3$ uniquely determine bandlimited structures (to be precisely defined in Section 2.1) when the viewing distribution ρ is the uniform distribution over all possible rotations. This has since been

[1]The complex conjugate in the last mode ensures symmetry properties of the second-order moment; some related work uses different conventions.

justified theoretically [4, 18, 17]. However, the sample complexity required to accurately estimate the dth-order moment scales as $\omega(\sigma^{2d})$ [4, 1], which becomes prohibitive even for the moderate value $d = 3$, when the noise variance σ^2 is high. Moreover, when representing the moments by discretized arrays, the associated storage and computational costs also scale exponentially in the order of the moments, which makes numerical operations challenging. One approach to mitigate these issues uses compressed low-rank tensor formats [22].

Much recent work has focused on improving techniques when using moments of only order $d = 2$, to circumvent the prohibitive complexities enocuntered for higher moment orders. A number of recent papers show that the second-order moment, under suitable conditions, identifies the molecular structure either uniquely [7, 26, 6, 5], or up to a finite list [34]. These results have been used numerically to produce ab-initio reconstructions that can be further improved using iterative refinement and to produce pseudo-metrics for directly comparing experimental cryo-EM images without the need for reconstruction [45]. A number of works have also been concerned with efficient numerical schemes [9, 23].

However, in order to obtain high-resolution reconstructions directly from the moments, a number of computational challenges still remain. A major difficulty stems from the non-convexity of the moment matching optimization problem, which makes it likely that iterative methods stagnate or converge to spurious local minima and therefore do not recover the exact ground truth structure.

1.3 Contributions

This paper overcomes previous computational obstacles in using the method-of-moments by considering two instances of moments, obtained through different distributions of rotations ρ, i.e., by assuming experimental access to the empirical moments

$$\widetilde{m}_2[\Phi, \rho_1], \qquad \text{and} \qquad \widetilde{m}_2[\Phi, \rho_2], \tag{1.5}$$

for two distinct distributions ρ_1 and ρ_2. These can be obtained by running two experiments and varying the experimental conditions between them, for instance by varying the tilt angle of the specimen with respect to the electron beam [2] or through laser flash melting [41] of the sample, or by adding charged detergents to the sample [27].

In the remainder of this paper, we make the assumption that ρ_1 is the uniform distribution over all rotations and that ρ_2 is *in-plane uniform*, meaning that the distribution of the resulting projection images is invariant to rotations of the image; see (2.6) for a definition. The second assumption can without loss of generality be achieved by augmenting the dataset with rotations of the obtained projection images. We aim to relax the first assumption in future work to instead only require that both ρ_1 and ρ_2 are in-plane uniform. Moreover, we will assume that ρ_2 is invariant to in plane reflections of the projection images through the origin, which can without loss of generality be achieved by augmenting the dataset with a copy of the reflected images.

We show that these two population moments together identify the molecular structure uniquely (rather than up to a finite list), provided the structure is bandlimited (see Section 2.4 for a precise statement). We also devise a numerical reconstruction algorithm, which we term the method-of-double-moments. Crucially, we demonstrate numerically that this method converges to the ground truth structure for bandlimited structures when using the population moments, apparently without stagnation or convergence to spurious local minima, which enables efficient reconstruction.

2 Preliminaries

2.1 Basis representation of structure

Assume the Fourier transformed volume $\widehat{\Phi}$ is a square-integrable function supported on a ball of radius $r_{\max}$. To find explicit representations of the population moments in (1.5), we represent $\widehat{\Phi}$ in spherical coordinates (r, θ, φ) using a spherical harmonics expansion for each fixed radius, i.e.,

$$\widehat{\Phi}(r, \theta, \varphi) = \sum_{\ell=0}^{L} \sum_{m=-\ell}^{\ell} A_{\ell m}(r) Y_\ell^m(\theta, \varphi), \quad r \in [0, r_{\max}], \quad \theta \in [0, \pi], \quad \varphi \in [0, 2\pi), \tag{2.1}$$

where Y_ℓ^m are the complex-valued spherical harmonics [15, Eq. 14.30.1], the positive integer L is a bandlimit parameter and $A_{\ell m}(r)$ is a scalar complex-valued function of r.

To motivate the validity of (2.1), note that the Dirichlet Laplacian on the ball of radius $r_{\max}$ has eigenfunctions $\psi_{k\ell m}(r, \theta, \phi) := j_\ell(\lambda_{\ell k} \frac{r}{r_{\max}}) Y_\ell^m(\theta, \varphi)$, where j_ℓ is the ℓth spherical Bessel function of the first kind and $\lambda_{\ell k}$ is its kth root [21, §3.3], with $k \in \mathbb{Z}_{>0}, \ell \in \mathbb{Z}_{\geq 0}$ and $m \in \{-\ell, \ldots, \ell\}$. The $\psi_{k\ell m}$'s therefore form a complete orthonormal basis for the space of square-integrable functions on the ball. By summing the $\psi_{k\ell m}$'s over the index k, it follows that any square-integrable function supported on the ball of radius $r_{\max}$ can be represented in the form in (2.1) as we let $L \to \infty$.

Here we assume that $\widehat{\Phi}$ is bandlimited, in the sense that $\widehat{\Phi}$ can be represented exactly in the form in (2.1) for a finite value of L. Although this is an idealization, should this not hold, higher components $A_{\ell m}(r) Y_\ell^m(\theta, \Phi)$ for $\ell > L$ can be treated as an additional source of approximation error.

Section (2.3) presents explicit analytical expressions for the moment $m_2[\Phi, \rho]$ for bandlimited functions of the form (2.1), using the complex-valued spherical harmonics introduced above. When describing our algorithm, it will however be convenient to also use real-valued spherical harmonics. We therefore introduce notation for converting complex-valued spherical harmonics basis coefficients into coefficients in the real-valued spherical harmonics basis.

For each $\ell \in \mathbb{Z}_{\geq 0}$, write $Q_\ell \in \mathbb{C}^{(2\ell+1)\times(2\ell+1)}$ as a unitary matrix that has non-zero entries only on the main diagonal and anti-diagonal, with non-zero components defined explicitly by

$$(Q_\ell)_{mm} = \begin{cases} \mathbf{i}/\sqrt{2}, & \text{if } m < 0, \\ 1 & \text{if } m = 0, \\ (-1)^m/\sqrt{2}, & \text{if } m > 0, \end{cases} \qquad (Q_\ell)_{-m,m} = \begin{cases} 1/\sqrt{2}, & \text{if } m < 0, \\ 1 & \text{if } m = 0, \\ -(-1)^m \mathbf{i}/\sqrt{2}, & \text{if } m > 0, \end{cases} \tag{2.2}$$

for all $-\ell \le m \le \ell$. We denote by $\check{Y}_\ell^m(\theta,\varphi)$ the real-valued spherical harmonics defined by the convention

$$\check{Y}_\ell^m(\theta,\varphi) = \sum_{m'=-\ell}^{\ell} (Q_\ell)_{m,m'} Y_\ell^{m'}(\theta,\varphi), \tag{2.3}$$

where the real-valuedness of $\check{Y}_\ell^m$ follows from [15, Eq. 14.30.1, Eq. 14.9.3]. By changing the angular basis to $\check{Y}_\ell^m(\theta,\varphi)$, we can equivalently write (2.1) as

$$\widehat{\Phi}(r,\theta,\varphi) = \sum_{\ell=0}^{L} \sum_{m=-\ell}^{\ell} \check{A}_{\ell m}(r) \check{Y}_\ell^m(\theta,\varphi), \tag{2.4}$$

where

$$\check{A}_{\ell m}(r) = \sum_{m'=-\ell}^{\ell} A_{\ell m'}(r) (\overline{Q}_\ell)_{mm'}.$$

It is equivalent and more convenient to write in the opposite direction that

$$A_{\ell m}(r) = \sum_{m'=-\ell}^{\ell} \check{A}_{\ell m'}(r) (Q_\ell)_{m'm}, \tag{2.5}$$

which can explicitly be written out as

$$A_{\ell m}(r) = \begin{cases} \frac{\mathbf{i}}{\sqrt{2}} \check{A}_{\ell m}(r) + \frac{1}{\sqrt{2}} \check{A}_{\ell,-m}(r), & \text{if } m < 0, \\ \check{A}_{\ell 0}, & \text{if } m = 0, \\ \frac{-(-1)^m \mathbf{i}}{\sqrt{2}} \check{A}_{\ell,-m}(r) + \frac{(-1)^m}{\sqrt{2}} \check{A}_{\ell m}(r), & \text{if } m > 0. \end{cases}$$

Remark 2.1. For real-valued structures Φ, symmetry properties of the Fourier transform imply that the coefficients $\{\check{A}_{\ell m}(r) : -\ell \le m \le \ell\}$ are real for even ℓ and purely imaginary for odd ℓ [7].

2.2 Basis representation of rotational distribution

We will model the distribution of viewing orientations as having a density function $\rho(R)$ with respect to the uniform/Haar measure over the rotational group $\mathsf{SO}(3)$. We call a rotational distribution *in-plane uniform* or invariant to in-plane rotations if

$$\rho(R) = \rho(Rz(\alpha)) \tag{2.6}$$

for all $R \in \mathsf{SO}(3)$ and rotations $z(\alpha)$ of $\alpha \in \mathbb{R}$ radians around the z-axis. This results in the distribution of the projection images invariant to 2D rotations of the image.

We show in Appendix A.1 that any square-integrable density $\rho(R)$ inducing an in-plane uniform distribution of viewing rotations (of the tomographic projection images) can be written in the form

$$\rho(R)\mathrm{d}R = \sum_{p=0}^{\infty} \sum_{u=-p}^{p} B_{p,u} U_{u0}^p(R) \mathrm{d}R. \tag{2.7}$$

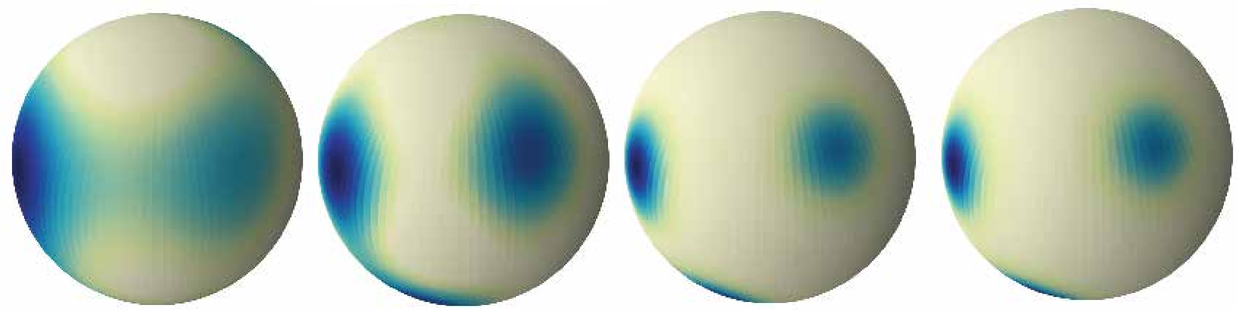

Figure 2.1: Illustration of the basis expansion of (2.7) as function of $\theta(R)$ and $\varphi(R)$, using $P = 3, 5, 10$ from leftmost to second-most right figure, and the rightmost figure as the ground-truth.

Here, $B_{p,u}$ are complex-valued basis coefficients, $\mathrm{d}R$ denotes the uniform distribution, i.e., $\int_{\mathsf{SO}(3)} \mathrm{d}R = 1$, and $U^p_{u0}(R)$ corresponds to the entries in the Wigner U-matrices having the closed-form expression [14, Eq. 9.42]

$$U^p_{u0}(R) = (-1)^u \sqrt{\frac{4\pi}{2p+1}} \overline{Y^u_p\left(\theta(R), \varphi(R)\right)}, \tag{2.8}$$

where $\theta(R)$ and $\varphi(R)$ are the angles in spherical coordinates of the last column vector of the rotation matrix R, i.e., the angles in spherical coordinates of the vector $(R_{1,3}, R_{2,3}, R_{3,3})$. By the orthogonality of the matrix elements $\{U^p_{uv}(R) : p \geq 0, -p \leq u, v \leq p\}$ [14, Eq. 9.32],

$$B_{p,u} = (2p+1) \cdot \int_{\mathsf{SO}(3)} \rho(R) \overline{U^p_{u0}}(R) dR \approx (2p+1) \cdot \frac{1}{N} \sum_{i=1}^{N} \rho(R_i) \overline{U^p_{u0}}(R_i)$$

where the R_i's are uniformly sampled i.i.d. over $\mathsf{SO}(3)$ or

$$B_{p,u} \approx (2p+1) \cdot \frac{1}{N} \sum_{i=1}^{N} \overline{U^p_{u0}}(R_i)$$

where the R_i's are drawn i.i.d. according to the distribution ρ.

The conditions that the density $\rho(R)$ is real-valued and that the integral of the density function equals one, translate into

$$\overline{B_{p,u}} = (-1)^u B_{p,-u}, \quad \text{and} \quad B_{0,0} = 1, \tag{2.9}$$

respectively, on the level of the coefficients (see Appendix A.1).

Moreover, the assumption that ρ is invariant to in-plane reflections of the projection images through the origin is equivalent (see Appendix A.1) to imposing

$$B_{p,u} = 0, \qquad \text{for } p \text{ odd}. \tag{2.10}$$

2.3 Explicit moment expressions

We show in Appendix A.2.2 that the second-order population moment (1.4) for a bandlimited structure of the form (2.1) with a rotational distribution of the form (2.7), has a succinct form. To present it, denote by $A_\ell : [0, r_{\max}] \to \mathbb{C}^{1\times(2\ell+1)}$, for $\ell \in \{0, \ldots, L\}$, $n \in \{-L, \ldots, L\}$ the row-vector-valued function defined by

$$A_\ell(r) = \left[A_{\ell,-\ell}(r), \quad A_{\ell,-\ell+1}(r), \quad \cdots, \quad A_{\ell,\ell}(r)\right], \tag{2.11}$$

and define the matrix $\mathcal{B}^n_{\ell,\ell'} \in \mathbb{C}^{(2\ell+1)\times(2\ell'+1)}$, for $\ell, \ell' \in \{0, \ldots, L\}$, $n \in \{-L, \ldots, L\}$, by

$$(\mathcal{B}^n_{\ell,\ell'})_{m,m'} = (-1)^{m+n}\mathcal{N}^n_\ell \mathcal{N}^n_{\ell'} \sum_{\ell''=\max\{|m-m'|,|\ell-\ell'|\}}^{\min\{\ell+\ell',P\}} \frac{\mathcal{C}_{\ell''}(\ell,\ell',m,-m',n,-n)}{2\ell''+1} B_{\ell'',m'-m}, \tag{2.12}$$

for $-\ell \le m \le \ell$ and $-\ell' \le m' \le \ell'$. Here, the scalar $\mathcal{N}^n_\ell \in \mathbb{R}$ is defined by

$$\mathcal{N}^n_\ell = N^n_\ell \cdot \mathbf{1}_{\{\ell \equiv n \pmod 2\}} \cdot \mathbf{1}_{\{\ell \ge |n|\}}, \tag{2.13}$$

where

$$N^n_\ell = \sqrt{\frac{2\ell+1}{4\pi}}\sqrt{\frac{(\ell-n)!}{(\ell+n)!}} \cdot P^n_\ell(0),$$

with $P^n_\ell(x)$ denoting the associated Legendre functions, [15, Eq. (14.3.6)]. The $\mathcal{C}_{\ell''}$ are septuply indexed constants defined (for general indices) by

$$\mathcal{C}_{\ell''}(\ell,\ell',m,m',n,n') := C(\ell,m;\ell',m'|\ell'',m+m')C(\ell,n;\ell',n'|\ell'',n+n'), \tag{2.14}$$

where the $C(\cdot,\cdot;\cdot,\cdot|\cdot,\cdot)$ are Clebsch-Gordan coefficients [14, Section 9.9].

Proposition 2.2. *The second-order population moment* (1.4) *for a bandlimited structure of the form* (2.1) *with a rotational distribution of the form* (2.7) *can be written as*

$$m_2(r,\varphi,r',\varphi') = \sum_{n=-L}^{L} e^{\mathbf{i}n(\varphi-\varphi')} \sum_{0\le\ell\le L}\sum_{0\le\ell'\le L} A_\ell(r)\mathcal{B}^n_{\ell,\ell'}(A_{\ell'}(r'))^{\mathsf{H}}. \tag{2.15}$$

In particular, $\mathcal{B}^n_{\ell,\ell'}$ *satisfies the Hermitian property* $\mathcal{B}^n_{\ell,\ell'} = (\mathcal{B}^n_{\ell',\ell})^{\mathsf{H}}$. *Also,* $\mathcal{B}^n_{\ell,\ell'} = 0$ *for any* $-L \le n \le L$ *whenever* $\ell \not\equiv \ell'$ *(mod 2).*

The proof is given in Appendix A.2.2. In particular, for a uniform distribution of rotations, $B_{\ell,m} = 0$ unless $\ell = 0$ and $m = 0$, so (2.15) simplifies to

$$m_2(r,r',\psi) = 4\pi \sum_{\ell=0}^{L}\sum_{m=-\ell}^{\ell} A_{\ell m}(r)\overline{A_{\ell,m}(r')}P_\ell\left(\cos(\psi)\right), \tag{2.16}$$

after using the addition theorem for spherical harmonics [14, Eqn. 4.37], where the P_ℓ are the Legendre polynomials [15, §18.3], and $\psi := \varphi - \varphi'$.

2.4 Precise problem statement

With the notation from the previous sections, we can now formally state our problem. We make the following assumptions.

Assumption 2.3. (Assumptions on the structure Φ and the distributions ρ_1, ρ_2)

1. Φ is bandlimited with respect to its angular variables, i.e., Φ can be expressed as in (2.1) for some $L \in \mathbb{Z}$. Moreover, $L \geq 3$.

2. The radial functions $(A_{\ell,m}(r) : 0 \leq \ell \leq L, -\ell \leq m \leq \ell)$ in (2.1) are linearly independent.

3. ρ_1 is the uniform Haar measure on $\mathsf{SO}(3)$.

4. ρ_2 is in-plane uniform, i.e., the distribution of the projection images obtained from ρ_2 are invariant to in-plane rotations. The distribution ρ_2 is also invariant to in-plane reflections of the projection images through the origin. Moreover, $P \geq 2L$ and the following expansion coefficients of ρ_2 from (2.7) are Zariski-generic:

$$(B_{p,u} : 1 \leq p \leq 2L, p \text{ is even}, -p \leq u \leq p) \in \mathbb{C}^{2L^2+3L}.$$

Problem 2.4. Let Φ, ρ_1, ρ_2 satisfy Assumption 2.3. Given samples of $\widetilde{m}_1[\Phi, \rho_1]$, $\widetilde{m}_2[\Phi, \rho_1]$ and $\widetilde{m}_2[\Phi, \rho_2]$ on a grid in polar coordinates defined by

$$\{r_1, \ldots, r_{N_r}\} \subseteq [0, r_{\max}], \qquad \{\varphi_1, \ldots, \varphi_{N_\varphi}\} \subseteq [0, 2\pi), \tag{2.17}$$

determine the structure Φ.

3 Main theoretical result

We next state the main theoretical result of this paper. The theorem ensures that the first and second population moments generically uniquely identify the structure Φ and nonuniform distribution (suitably low-passed), which justifies the computational problem in Problem 2.4. Denote by $\rho_2^{\downarrow 2L}$ the low-pass of ρ_2 to degree $2L$, i.e., (2.7) truncated to $p \leq 2L$.

Theorem 3.1. *If Φ, ρ_1, and ρ_2 satisfy Assumption 2.3, then $m_1[\Phi, \rho_1]$, $m_2[\Phi, \rho_1]$ and $m_2[\Phi, \rho_2]$ uniquely identify Φ and $\rho_2^{\downarrow 2L}$ up to the action of $\mathsf{SO}(3)$ on $(\Phi, \rho_2^{\downarrow 2L})$ and up to chirality.*

The proof is presented in Section 5.

Remark 3.2. Theorem 3.1 identifies the structure up to an overall global rotation and reflection, which is an unavoidable ambiguity in cryo-EM, and therefore not a drawback of this particular result.

Remark 3.3. We will show Theorem 3.1 by induction on L, with the verification of the base case $L = 3$ requiring computer assistance. Specifically, we use floating-point arithmetic and pseudo-random numbers for the base cases. While this is standard practice in computational algebra, it falls short of providing a completely rigorous proof; thus the proof of Theorem 3.1 in Section 5 is labeled as a "Computational Proof". All other steps in the argument are rigorous.

Remark 3.4. The uniqueness theorem implies a provable polynomial time algorithm for inverting the population moments provided Assumption 2.3 holds. However we develop a different numerical method in the next section, which doesn't rely on frequency marching and polynomial system solving and hence is less susceptible to noise.

We prove Theorem 3.1 in section 5. Section 4 presents the main computational result: an algorithm for solving Problem 2.4 given access only to discrete samples of the sample moments.

4 Algorithm: the method-of-double-moments

This section details the computational algorithm used to solve Problem 2.4. The method consists of three steps:

1. Use the uniform sample moment $\widetilde{m}_2[\Phi, \rho_1]$ to determine the coefficients $A_\ell(r_i)$ for $i = 1, \dots, N_r$, up to the action of unknown orthogonal matrices $O_\ell \in \mathsf{O}(2\ell + 1)$ for $\ell = 0, \dots, L$.

2. Use the in-plane uniform sample moment $\widetilde{m}_2[\Phi, \rho_2]$ to formulate a non-linear optimization problem in the variables O_ℓ and $B_{p,u}$.

3. Solve the optimization problem through an alternating procedure solving iteratively and repeatedly for O_ℓ and $B_{p,u}$ in turn.

These steps are detailed in Sections 4.1 – 4.3, respectively, and a summary of the method is provided in Algorithm 1.

4.1 Step 1: using the uniform sample moment

It follows from (2.16) and orthogonality properties of P_ℓ that

$$C_\ell(r, r') := \frac{2\ell + 1}{4\pi} \int_0^\pi m_2[\Phi, \rho_1](r, r', \psi) P_\ell(\cos\psi) \sin(\psi) d\psi = \sum_{m=-\ell}^{\ell} A_{\ell m}(r) \overline{A_{\ell m}(r')}, \quad (4.1)$$

for a uniform distribution ρ_1, which yields partial information about the unknown coefficients $A_{\ell m}$.

Assume we have access to samples on the grid in (2.17). We approximate the integral in (4.1) by firstly using the sample moment $\widetilde{m}_2[\Phi, \rho_1]$ instead of the population moment,

Algorithm 1: The method-of-double-moments

Input: Sample moments $\widetilde{m}_2[\Phi,\rho_1]$ and $\widetilde{m}_2[\Phi,\rho_2]$ satisfying Assumption 2.3 and sampled on the grid (2.17), maximum number of iterations K

Result: Approximation $\Phi^{(K)}$ to the molecular structure Φ

Compute $\widetilde{C}$ in (4.2) through numerical quadrature `/* Step 1 */`

Compute $\widetilde{A}$ in (4.5) through the Cholesky decomposition of $\widetilde{C}$

Compute G_n in (4.9) through numerical quadrature `/* Step 2 */`

Compute $\mathcal{M}^n$ in (4.12) by left- and right-multiplying G_n by $\widetilde{A}^{\dagger}$ and $\widetilde{A}^{\mathsf{H},\dagger}$, respectively.

Compute iterative solutions $O_\ell^{(k)}$ and $B_{p,u}^{(k)}$ to the update equations (4.19) – (4.21), for $k = 1,\ldots,K$. `/* Step 3 */`

Return the inverse discrete Fourier transform of

$$\widehat{\Phi}^{(K)}(r_i,\theta,\varphi) := \sum_{\ell=0}^{L}\sum_{m=-\ell}^{\ell}(\widetilde{A}_\ell O_\ell^{(K)})_{i,m}\check{Y}_\ell^m(\theta,\varphi),$$

sampled at the radial points r_i from (2.17) for $i = 1,\ldots,N_r$.

and secondly by using numerical quadrature with quadrature points φ_s,φ_q and quadrature weights $w_{s,q}$, for $s,q = 0,\ldots,N_\varphi$, i.e., we compute

$$\widetilde{C}_\ell(r_i,r_j) := \frac{2\ell+1}{4\pi}\sum_{s,q=0}^{N_\varphi} w_{s,q}\widetilde{m}_2[\Phi,\rho_1](r_i,r_j,\varphi_s-\varphi_q)P_\ell(\cos(\varphi_s-\varphi_q))\sin(\varphi_s-\varphi_q). \quad (4.2)$$

Next, denote by $A_\ell \in \mathbb{C}^{N_r\times(2\ell+1)}$, $\check{A}_\ell \in \mathbb{C}^{N_r\times(2\ell+1)}$ and $\widetilde{C}_\ell \in \mathbb{C}^{N_r\times N_r}$ the matrices defined by

$$(A_\ell)_{k,m} = A_{\ell m}(r_k), \qquad (\check{A}_\ell)_{k,m} = \check{A}_{\ell m}(r_k), \qquad (\widetilde{C}_\ell)_{i,j} = \widetilde{C}_\ell(r_i,r_j). \quad (4.3)$$

Inserting these definitions into (4.1) and (4.2) gives

$$\widetilde{C}_\ell \approx A_\ell A_\ell^{\mathsf{H}} = \check{A}_\ell\check{A}_\ell^{\mathsf{H}}, \quad (4.4)$$

where the approximate equality comes from discretization errors and the equality from (2.5) together with orthogonality of the Q_ℓ.

We next compute the Cholesky decomposition of the matrices $\widetilde{C}_\ell$, ignore the discretization and sample errors in (4.4) and use the fact that $\check{A}_\ell$ is real for even ℓ and purely imaginary for odd ℓ, from Section 2.1. This yields the matrices

$$\widetilde{A}_\ell := \check{A}_\ell O_\ell^{\mathsf{T}} = A_\ell Q_\ell^{\mathsf{H}} O_\ell^{\mathsf{T}}, \quad (4.5)$$

for each $0 \le \ell \le L$, where the $O_\ell \in \mathsf{O}(2\ell+1)$ are unknown and real-valued orthogonal matrices.

4.2 Step 2: using the non-uniform sample moment

The remainder of the computational method attempts to determine the matrices O_ℓ, for $0 \le \ell \le L$ by matching the additional sample moment $\widetilde{m}_2[\Phi,\rho_2]$ to the corresponding population moment. We therefore re-express $m_2[\Phi,\rho_2]$ in terms of the matrices $\widetilde{A}_\ell$ computed in Section 4.1. Inserting (4.5) into (A.15) gives

$$m_2(r,\varphi,r',\varphi') = \sum_{n=-L}^{L} e^{in(\varphi-\varphi')} \sum_{\ell=0}^{L}\sum_{\ell'=0}^{L} \widetilde{A}_\ell(r) O_\ell Q_\ell \mathcal{B}^n_{\ell,\ell'} Q^{\mathsf{H}}_{\ell'} O^{\mathsf{T}}_{\ell'} (\widetilde{A}_{\ell'}(r'))^{\mathsf{H}}. \tag{4.6}$$

Note that

$$\frac{1}{(2\pi)^2}\int_0^{2\pi}\int_0^{2\pi} m_2[\Phi,\rho_2](r,\varphi,r',\varphi') e^{-in(\varphi-\varphi')}\mathrm{d}\varphi \mathrm{d}\varphi' = \sum_{\ell=0}^{L}\sum_{\ell'=0}^{L} \widetilde{A}_\ell(r) O_\ell Q_\ell \mathcal{B}^n_{\ell,\ell'} Q^{\mathsf{H}}_{\ell'} O^{\mathsf{T}}_{\ell'} (\widetilde{A}_{\ell'}(r'))^{\mathsf{H}}. \tag{4.7}$$

Approximating the integral by firstly using the sample moment $\widetilde{m}_2[\Phi,\rho_2]$ and secondly by using numerical quadrature yields

$$\begin{aligned} g_n(r_i,r_j) &:= \frac{1}{(2\pi)^2}\sum_{s,q=0}^{N_\varphi} w_{s,q} \widetilde{m}_2[\Phi,\rho_2](r_i,r_j,\varphi_s-\varphi_q) e^{-in(\varphi_s-\varphi_q)} \\ &\approx \sum_{\ell,\ell'=0}^{L} \widetilde{A}_\ell(r_i) O_\ell Q_\ell \mathcal{B}^n_{\ell,\ell'} Q^{\mathsf{H}}_{\ell'} O^{\mathsf{T}}_{\ell'} (\widetilde{A}_{\ell'}(r_j))^{\mathsf{H}}, \end{aligned} \tag{4.8}$$

for each $-L \le n \le L$ and where the approximate equality comes from discretization and sample errors.

Write $G_n \in \mathbb{C}^{N_r\times N_r}$ and $\mathcal{M}^n_{\ell,\ell'} \in \mathbb{C}^{(2\ell+1)\times(2\ell'+1)}$ as the matrices defined by

$$(G_n)_{i,j} = g_n(r_i,r_j), \quad \text{and} \quad \mathcal{M}^n_{\ell,\ell'} = O_\ell Q_\ell \mathcal{B}^n_{\ell,\ell'} Q^{\mathsf{H}}_{\ell'} O^{\mathsf{T}}_{\ell'}, \tag{4.9}$$

and define $\mathcal{M}^n$ and $\mathcal{B}^n \in \mathbb{C}^{(L+1)^2\times(L+1)^2}$ to be the block matrices with (ℓ,ℓ')-th block $\mathcal{M}^n_{\ell,\ell'}$ and $\mathcal{B}^n_{\ell,\ell'}$, respectively, i.e.,

$$\mathcal{M}^n = \begin{bmatrix} \mathcal{M}^n_{0,0} & \mathcal{M}^n_{0,1} & \cdots & \mathcal{M}^n_{0,L} \\ \mathcal{M}^n_{1,0} & \mathcal{M}^n_{1,1} & \cdots & \mathcal{M}^n_{1,L} \\ \vdots & \vdots & \ddots & \vdots \\ \mathcal{M}^n_{L,0} & \mathcal{M}^n_{L,1} & \cdots & \mathcal{M}^n_{L,L} \end{bmatrix}, \quad \text{and} \quad \mathcal{B}^n = \begin{bmatrix} \mathcal{B}^n_{0,0} & \mathcal{B}^n_{0,1} & \cdots & \mathcal{B}^n_{0,L} \\ \mathcal{B}^n_{1,0} & \mathcal{B}^n_{1,1} & \cdots & \mathcal{B}^n_{1,L} \\ \vdots & \vdots & \ddots & \vdots \\ \mathcal{B}^n_{L,0} & \mathcal{B}^n_{L,1} & \cdots & \mathcal{B}^n_{L,L} \end{bmatrix}. \tag{4.10}$$

Further write $\widetilde{A} \in \mathbb{C}^{N_r\times(L+1)^2}$ as the block matrix with ℓ-th block $\widetilde{A}_\ell \in \mathbb{C}^{N_r\times(2\ell+1)}$, i.e.,

$$\widetilde{A} = \begin{bmatrix} \widetilde{A}_0 & \cdots & \widetilde{A}_L \end{bmatrix}.$$

Ignoring quadrature errors, we can then write (4.8) in the matrix form

$$G_n = \widetilde{A}\mathcal{M}^n\widetilde{A}^{\mathsf{H}}. \tag{4.11}$$

Assuming $\widetilde{A}$ has full rank (which in particular requires that $N_r \geq (L+1)^2$), we can left- and right-multiply this equation by $\widetilde{A}^\dagger$ and $\widetilde{A}^{\mathsf{H},\dagger}$ to obtain approximate access to $\mathcal{M}^n$. Writing

$$O = \mathrm{blockdiag}_{\ell=0,\ldots,L}(O_\ell), \quad \text{and} \quad Q = \mathrm{blockdiag}_{\ell=0,\ldots,L}(Q_\ell),$$

we can write this as

$$\widetilde{A}^\dagger G_n \widetilde{A}^{\mathsf{H},\dagger} = \mathcal{M}^n = OQ\mathcal{B}^n Q^{\mathsf{H}} O^{\mathsf{T}}, \quad \text{for} \quad -L \leq n \leq L. \tag{4.12}$$

4.3 Step 3: alternating optimization

We solve equations (4.12) through an alternating procedure for the matrices O_ℓ and the parameters $B_{p,u}$, by initializing $O_\ell^{(0)}$ as arbitrary orthogonal matrices and updating the parameters $B_{p,u}^{(k)}$ and $O_\ell^{(k)}$ iteratively, for $k = 0, \ldots, K$.

4.3.1 Solving for $B_{p,u}$

The update equation for $B_{p,u}$ proceeds by minimizing the expression

$$\sum_{n=-L}^{L} \|\mathcal{M}^n - O^{(k)}Q\mathcal{B}^n Q^{\mathsf{H}} O^{(k),T}\|^2, \tag{4.13}$$

in the variables $B_{p,u}$ while imposing the constraints (2.9), i.e., by restricting B to the set

$$\mathcal{S}_{\mathcal{B}} := \left\{(B_{p,u})_{(p,u)\in\mathcal{I}} : B_{p,u} \in \mathbb{C}, \quad \overline{B_{p,u}} = (-1)^u B_{p,-u}, \quad B_{0,0} = 1\right\}, \tag{4.14}$$

where $\mathcal{I} := \{(p,u) \subseteq \mathbb{Z}_{\geq 0} \times \mathbb{Z} : -p \leq u \leq p\}$. Note that the constraint set $\mathcal{S}_{\mathcal{B}}$ does not impose positivity of the resulting density in (2.7), for simplicity. This can however be incorporated by, for instance, requiring positivity at a given set of collocation points R_i (see [34, Eq. (51)]). This yields the constraints $\rho(R_i) \geq 0$, which are linear constraints in the variables $B_{p,u}$ and therefore can be included when minimizing (4.13), although at the expense of increased runtime.

4.3.2 Solving for O_ℓ

The update for O_ℓ proceeds by a relaxed procedure, where we first note that

$$\|\mathcal{M}^n - OQ\mathcal{B}^{n,k}Q^{\mathsf{H}}O^T\| = \|\mathcal{M}^n O - OQ\mathcal{B}^{n,k}Q^{\mathsf{H}}\|, \tag{4.15}$$

where $\mathcal{B}^{n,k}$ is the matrix in (4.10) formed from the coefficients $B_{p,u}^{(k)}$. Relaxing the orthogonality constraint of O, we can solve this least-squares problem and then orthogonalize the result. We will solve this relaxed least-squares problem over the following constraint set:

$$\mathcal{S}_{\mathcal{X}} = \left\{ \text{blockdiag}_{\ell=0,\ldots,L}(X_\ell) : X_\ell \in \mathbb{R}^{(2\ell+1)\times(2\ell+1)}, \quad X_0 = 1, \quad X_1 = I_3 \right\}. \tag{4.16}$$

We can restrict the search to the set $\mathcal{S}_{\mathcal{X}}$, because for any choice of X_0 and X_1, there is a choice of rotation of the structure Φ that jointly maps X_0 to 1 and X_1 to I_3.

Given X, we orthogonalize the result by projecting X onto the set

$$\mathcal{S}_{\mathcal{O}} = \left\{ \text{blockdiag}_{\ell=0,\ldots,L}(O_\ell) : O_\ell \in \mathsf{O}(2\ell+1) \right\}, \tag{4.17}$$

i.e., by minimizing

$$\|O - X\| = \sum_{\ell=0}^{L} \|O_\ell - X_\ell\|^2, \tag{4.18}$$

where the equality comes from the block-diagonal structure of X and O.

4.3.3 Summary

Taken together, the update equations for B and O can be written as

$$B^{(k+1)} = \operatorname*{arg\,min}_{B\in\mathcal{S}_{\mathcal{B}}} \sum_{n=-L}^{L} \|\mathcal{M}^n - O^{(k)} Q \mathcal{B}^n Q^{\mathsf{H}} O^{(k),T}\|^2, \tag{4.19}$$

$$X^{(k+1)} = \operatorname*{arg\,min}_{X\in\mathcal{S}_{\mathcal{X}}} \sum_{n=-L}^{L} \|\mathcal{M}^n X - X Q \mathcal{B}^{n,(k)} Q^{\mathsf{H}}\|^2, \tag{4.20}$$

$$O^{(k+1)} = \operatorname*{arg\,min}_{O\in\mathcal{S}_{\mathcal{O}}} \sum_{\ell=0}^{L} \|O_\ell - X_\ell^{(k+1)}\|^2. \tag{4.21}$$

Equations (4.19) and (4.20) are structured least squares-problems in the variables $B_{p,u}$ and X_ℓ, respectively, and can be solved efficiently. The orthogonalization procedure in equation (4.21) is a sequence of $L+1$ orthogonal Procrustes problems, which can be solved in closed form by computing singular value decompositions of the diagonal blocks $X_\ell^{(k+1)}$ [33].

5 Proof of Theorem 3.1

The next lemma establishes basic symmetries of Problem 2.4. These correspond to the well-known fact that structures in cryo-EM can only ever be recovered up to rotation and reflection.

Lemma 5.1. *Let Φ, ρ_1, ρ_2 and $\tilde{\Phi}, \rho_1, \tilde{\rho}_2$ both satisfy satisfy Assumption 2.3. Assume they differ from each other by a global rotation and possibly chirality, that is, there exist $S \in \mathsf{SO}(3)$ and $\epsilon \in \{0,1\}$ such that for all $\mathbf{x} \in \mathbb{R}^3$ and $R \in \mathsf{SO}(3)$ it holds*

$$\tilde{\Phi}(\mathbf{x}) = \Phi(J^\epsilon S \mathbf{x}) \qquad \textit{and} \qquad \tilde{\rho}_2(R) = \rho_2(J^\epsilon S R J^\epsilon), \tag{5.1}$$

where $J = \operatorname{diag}(1,1,-1)$. Then we have

$$m_1[\Phi, \rho_1] = m_1[\tilde{\Phi}, \rho_1], \quad m_2[\Phi, \rho_1] = m_2[\tilde{\Phi}, \rho_1], \quad \textit{and} \quad m_2[\Phi, \rho_2] = m_2[\tilde{\Phi}, \tilde{\rho}_2]. \tag{5.2}$$

Proof. In fact, we claim that the distributions of tomographic projection images I_R with noise removed (that is, (1.2) without the $\varepsilon(x,y)$ term) as generated by (Φ, ρ_1) and (Φ, ρ_2) match the distributions generated by $(\tilde{\Phi}, \rho_1)$ and $(\tilde{\Phi}, \tilde{\rho}_2)$, respectively. Consequently, $m_k[\Phi, \rho_1] = m_k[\tilde{\Phi}, \rho_1]$ and $m_k[\Phi, \rho_2] = m_k[\tilde{\Phi}, \tilde{\rho}_2]$ for all $k \geq 1$. In particular, (5.2) holds as wanted.

Let us now justify the claim. First compare (Φ, ρ_2) and $(\tilde{\Phi}, \tilde{\rho}_2)$. Under $(\tilde{\Phi}, \tilde{\rho}_2)$, the distribution of noiseless tomographic projection images draws with density $\tilde{\rho}_2(R) = \rho_2(J^\epsilon S R J^\epsilon)$,

$$\int_{-\infty}^{\infty} (R^\top \cdot \tilde{\Phi})(\mathbf{x}) dz \; = \; \int_{-\infty}^{\infty} \Phi(J^\epsilon S R \mathbf{x}) dz \; = \; \int_{-\infty}^{\infty} \Phi(J^\epsilon S R J^\epsilon J^\epsilon \mathbf{x}) dz \; = \; \int_{-\infty}^{\infty} \Phi(J^\epsilon S R J^\epsilon \mathbf{x}) dz, \tag{5.3}$$

where the last equality in (5.3) is by a change of variable replacing z by $(-1)^\epsilon z$. Meanwhile, under (Φ, ρ_2) the distribution of noiseless tomographic projection images draws

$$\int_{-\infty}^{\infty} \Phi(J^\epsilon S R J^\epsilon \mathbf{x}) dz, \tag{5.4}$$

with density $\rho_2(J^\epsilon S R J^\epsilon)$. The distributions are identical, as claimed. Comparing (Φ, ρ_1) and (Φ, ρ_1), the image distributions likewise are the same, because $\rho_1(R) = \rho_1(J^\epsilon S R J^\epsilon)$ since ρ_1 is the uniform distribution. This justifies our claim and finishes the proof of the lemma. □

Computational Proof of Theorem 3.1. Let Φ, ρ_1, and ρ_2 satisfy Assumption 2.3. Suppose $\tilde{\Phi}$ and $\tilde{\rho}_2$ are another structure and distribution with expansions

$$\widehat{\tilde{\Phi}}(r, \theta, \varphi) = \sum_{\ell=0}^{L} \sum_{m=-\ell}^{\ell} \tilde{A}_{\ell m}(r) Y_\ell^m(\theta, \varphi), \quad r \in [0, r_{\max}], \quad \theta \in [0, \pi], \quad \varphi \in [0, 2\pi), \tag{5.5}$$

and

$$\tilde{\rho}_2(R) \mathrm{d}R = \sum_{\substack{p=0 \\ p \text{ even}}}^{\infty} \sum_{u=-p}^{p} \tilde{B}_{pu} U_{u0}^p(R) \mathrm{d}R, \tag{5.6}$$

such that there is a matching of population moments:

$$m_1[\Phi, \rho_1] = m_1[\tilde{\Phi}, \rho_1], \quad m_2[\Phi, \rho_1] = m_2[\tilde{\Phi}, \rho_1], \quad m_2[\Phi, \rho_2] = m_2[\tilde{\Phi}, \tilde{\rho}_2]. \tag{5.7}$$

Our goal is to prove that $(\tilde{\Phi}, \tilde{\rho}_2^{\downarrow 2L})$ equals $(\Phi, \rho_2^{\downarrow 2L})$ up to rotation and possibly chirality. As in Lemma 5.1, this precisely means there exist $S \in \mathsf{SO}(3)$ and $\epsilon \in \{0,1\}$ such that $\tilde{\Phi}(\mathbf{x}) = \Phi(J^\epsilon S\mathbf{x})$ and $\tilde{\rho}_2^{\downarrow 2L}(R) = \rho_2^{\downarrow 2L}(J^\epsilon SRJ^\epsilon)$. Notice $\tilde{\Phi}(\mathbf{x}) = \Phi(J^\epsilon S\mathbf{x})$ is equivalent to

$$\tilde{A}_\ell(r) = A_\ell(r)U^\ell(J^\epsilon S), \quad \text{for all } 0 \le \ell \le L, \tag{5.8}$$

because

$$\widehat{\Phi}(J^\epsilon S\mathbf{x}) = \sum_{\ell=0}^{L}\sum_{m=-\ell}^{\ell} A_{\ell m}(r)\sum_{n=-\ell}^{\ell} U^\ell_{mn}(J^\epsilon S)Y_\ell^n(\theta,\varphi) = \sum_{\ell=0}^{L}\sum_{m=-\ell}^{\ell}[A_\ell(r)U^\ell(J^\epsilon S)]_m Y_\ell^m(\theta,\varphi).$$

Toward this goal, we first use the condition $m_2[\Phi,\rho_1] = m_2[\tilde{\Phi},\rho_1]$. By [24], it implies

$$\tilde{A}_\ell(r) = A_\ell(r)Q_\ell^{\mathsf{H}}O_\ell^{\mathsf{T}}Q_\ell, \quad \text{for all } 0 \le \ell \le L, \tag{5.9}$$

where $O_\ell \in \mathbb{R}^{(2\ell+1)\times(2\ell+1)}$ are some unknown real-valued orthogonal matrices and $Q_\ell \in \mathbb{C}^{(2\ell+1)\times(2\ell+1)}$ are the complex-valued unitary matrices (2.2). Next, we use $m_1[\Phi,\rho_1] = m_1[\tilde{\Phi},\rho_1]$. This implies $\tilde{A}_0(r) = A_0(r)$, again by [24]. Since $Q_0^{\mathsf{H}} = 1$ it follows that

$$O_0 = 1, \tag{5.10}$$

where $O_0 \in \mathbb{R}$ is the 1×1 orthogonal matrix in (5.9).

Next, we claim that by the symmetry in (5.8), it is without loss of generality to assume

$$O_1 = I \in \mathbb{R}^{3\times 3}. \tag{5.11}$$

Indeed, if $O_1 \neq I$ there exist $S \in \mathsf{SO}(3)$ and $\epsilon \in \{0,1\}$ such that $Q_1^{\mathsf{H}}U^1(J^\epsilon S)Q_1 = O_1$ (see [14, pg. 324]). Then the replacement $\Phi(\mathbf{x}) \leftarrow \Phi(J^\epsilon S\mathbf{x})$ reduces us to $O_1 = I$ (cf. (5.9)). Note assuming $O_1 = I$ kills rotational and chiral ambiguities of the problem, i.e., it makes the goal to prove equalities on the nose, $\tilde{\Phi} = \Phi$ and $\tilde{\rho}_2 = \rho_2$. Thus with (5.11), we want

$$O_\ell = I, \qquad \text{for all } 0 \le \ell \le L, \text{ and} \tag{5.12}$$

$$\tilde{B}_{pu} = B_{pu}, \qquad \text{for all } 0 \le p \le 2L \text{ with } p \text{ even and } -p \le u \le p. \tag{5.13}$$

To show (5.12) and (5.13), we turn to the condition $m_2[\Phi,\rho_2] = m_2[\tilde{\Phi},\tilde{\rho}_2]$. First by A.15,

$$m_2[\Phi,\rho_2](r,\varphi,r',\varphi') = \sum_{n=-L}^{L} e^{\mathrm{i}n(\varphi-\varphi')}\sum_{\ell=0}^{L}\sum_{\ell'=0}^{L} A_\ell(r)\mathcal{B}^n_{\ell,\ell'}(A_{\ell'}(r'))^{\mathsf{H}}. \tag{5.14}$$

Combining with (5.9),

$$m_2[\tilde{\Phi},\tilde{\rho}_2](r,\varphi,r',\varphi') = \sum_{n=-L}^{L} e^{\mathrm{i}n(\varphi-\varphi')}\sum_{\ell=0}^{L}\sum_{\ell'=0}^{L} A_\ell(r)Q_\ell^{\mathsf{H}}O_\ell^{\mathsf{T}}Q_\ell\tilde{\mathcal{B}}^n_{\ell,\ell'}Q_{\ell'}^{\mathsf{H}}O_{\ell'}Q_{\ell'}(A_{\ell'}(r'))^{\mathsf{H}}. \tag{5.15}$$

Equating (5.14) and (5.15) and using orthonormality of the Fourier modes, deduce

$$\sum_{\ell=0}^{L}\sum_{\ell'=0}^{L} A_\ell(r)\mathcal{B}^n_{\ell,\ell'}(A_{\ell'}(r'))^{\mathsf{H}} = \sum_{\ell=0}^{L}\sum_{\ell'=0}^{L} A_\ell(r)Q_\ell^{\mathsf{H}}O_\ell^{\mathsf{T}}Q_\ell\tilde{\mathcal{B}}^n_{\ell,\ell'}Q_{\ell'}^{\mathsf{H}}O_{\ell'}Q_{\ell'}(A_{\ell'}(r'))^{\mathsf{H}} \tag{5.16}$$

for each n satisfying $-L \leq n \leq L$. By the assumed linear independence of the radial functions $A_{\ell,m}$ (i.e., the second item of Assumption 2.3), this implies

$$\mathcal{B}^n_{\ell,\ell'} = Q_\ell^{\mathsf{H}}O_\ell^{\mathsf{T}}Q_\ell\tilde{\mathcal{B}}^n_{\ell,\ell'}Q_{\ell'}^{\mathsf{H}}O_{\ell'}Q_{\ell'} \tag{5.17}$$

for each (n,ℓ,ℓ') with $-L \leq n \leq L$ and $0 \leq \ell,\ell' \leq L$. Here $\tilde{\mathcal{B}}^n_{\ell,\ell'}$ depends on $\tilde{B}_p$ as $\mathcal{B}^n_{\ell,\ell'}$ does on B_p.

In the rest of the proof, our strategy is to leverage (5.17) for (n,ℓ,ℓ') in an appropriate order to establish (5.12) and (5.13) by induction on L. Precisely, we induct on the following:

$$\begin{aligned}&\textit{Take Assumption 2.3. Then } (5.17) \textit{ for} -L \leq n \leq L \text{ and } 0 \leq \ell,\ell' \leq L, \textit{ together with}\\ &(5.10) \textit{ and } (5.11), \textit{ imply } O_\ell = I \textit{ for } 0 \leq \ell \leq L \textit{ and } \tilde{B}_p = B_p \textit{ for } p = 0,2,\ldots,2L.\end{aligned} \tag{5.18}$$

The induction amounts to showing that a polynomial system in O_ℓ and $\tilde{B}_p$ has a unique solution.

The base case of the induction is $L = 3$. By (2.9), (5.10) and (5.11), we know $B_0 = \tilde{B}_0$, $O_0 = 1$ and $O_1 = I$. We wish to show $\tilde{B}_2 = B_2$, $\tilde{B}_4 = B_4$, $\tilde{B}_6 = B_6$, $O_2 = I$ and $O_3 = I$. We will use equations (5.17) suitably rearranged, together with orthogonality constraints:

$$\begin{cases} Q_\ell^{\mathsf{H}}O_\ell Q_\ell\mathcal{B}^n_{\ell,\ell'}Q_{\ell'}^{\mathsf{H}}O_{\ell'}^{\mathsf{T}}Q_{\ell'} = \tilde{\mathcal{B}}^n_{\ell,\ell'} \\ O_2O_2^{\mathsf{T}} = O_2^{\mathsf{T}}O_2 = I \\ O_3O_3^{\mathsf{T}} = O_3^{\mathsf{T}}O_3 = I, \end{cases} \tag{5.19}$$

where in the first line $(n,\ell,\ell') \in \{(1,1,1),(0,2,0),(0,2,2),(1,3,1),(1,3,3),(3,3,3)\}$. Dropping reality constraints on O_ℓ and $\tilde{B}_p$, we view (5.19) as a parameterized polynomial system over $\mathbb{C}$: the variables are $(\tilde{B}_2,\tilde{B}_4,\tilde{B}_6,O_2,O_3) \in \mathbb{C}^{101}$, the parameters are $(B_2,B_4,B_6) \in \mathbb{C}^{27}$, and there are $(3\times 3)+(5\times 1)+(5\times 5)+(5\times 5)+(7\times 3)+(7\times 7)+(7\times 7)+(5\times 5)+(5\times 5)+(7\times 7)+(7\times 7) = 331$ equations. Note the equations are affine-quadratic or linear in the variables and affine-linear in the parameters. By general properties of parameterized polynomial systems over $\mathbb{C}$, there exists a nonempty Zariski-open subset $\mathcal{U} \subseteq \mathbb{C}^{27}$ such that for $(B_2,B_4,B_6) \in \mathcal{U}$ the solution set to (5.19) has the same "type" of irreducible decomposition in the sense of [40, Theorem A.14.10]. Therefore, if we show on a randomly-generated instance of (B_2,B_4,B_6) that the polynomial system (5.19) has a unique solution over $\mathbb{C}$, then "with probability 1" the system Zariski-generically has a unique solution over $\mathbb{C}$, which then must be the trivial solution $\tilde{B}_p = B_p$ for $p = 2,4,6$ and $O_\ell = I$ for $\ell = 2,3$. Checking polynomial systems on random instances is a standard approach in computational algebra; that said, Remark 3.3 applies.

Here we perform the check using the numerical homotopy continuation software [12]. We generate (B_2,B_4,B_6) using a random number generator. The system (5.19) is too big to directly input into the software, so we break up the computation. Firstly, using the top line of (5.19) when $(n, \ell, \ell') = (1,1,1)$ it follows by a linear solve or by Lemma 5.2 that $\tilde{B}_2 = B_2$. Secondly, we take $(n, \ell, \ell') = (0,2,0)$, which gives the equation $Q_2^{\mathsf{H}} O_2 Q_2 \mathcal{B}_{2,0}^0 = \mathcal{B}_{2,0}^0$ or

$$O_2 Q_2 \mathcal{B}_{2,0}^0 = Q_2 \mathcal{B}_{2,0}^0, \tag{5.20}$$

i.e., O_2 fixes a known vector. We find that the vector is non-isotropic, i.e., $(Q_2\mathcal{B}_{2,0}^0)^{\mathsf{T}}(Q_2\mathcal{B}_{2,0}^0) \neq 0$, so we can extend the vector suitably scaled to a complex orthogonal matrix, i.e., find $\tilde{O}_2^{\mathsf{T}} \in O(5,\mathbb{C})$ and $\lambda \in \mathbb{C}$ such that the leftmost column of $\tilde{O}_2^{\mathsf{T}}$ is $\lambda Q_2 \mathcal{B}_{2,0}^0$. Then $\tilde{O}_2^{\mathsf{T}} e_1 = \lambda Q_2 \mathcal{B}_{2,0}^0$ or $\lambda \tilde{O}_2 Q_2 \mathcal{B}_{2,0}^0 = e_1$, where e_1 is the first standard basis, and (5.20) can be rewritten as $(\tilde{O}_2 O_2 \tilde{O}_2^{\mathsf{T}})\lambda \tilde{O}_2 Q_2 \mathcal{B}_{2,0}^0 = \lambda \tilde{O}_2 Q_2 \mathcal{B}_{2,0}^0$ or

$$(\tilde{O}_2 O_2 \tilde{O}_2^{\mathsf{T}}) e_1 = e_1.$$

Using $(\tilde{O}_2 O_2 \tilde{O}_2^{\mathsf{T}})^{\mathsf{T}}(\tilde{O}_2 O_2 \tilde{O}_2^{\mathsf{T}}) = I$, it follows that $\tilde{O}_2 O_2 \tilde{O}_2^{\mathsf{T}} = 1 \oplus \tilde{\tilde{o}}_2$ for some $\tilde{\tilde{o}}_2 \in O(4,\mathbb{C})$, i.e., $\tilde{O}_2 O_2 \tilde{O}_2^{\mathsf{T}}$ is block-diagonal. Next, consider $(n,\ell,\ell') = (0,2,2), (2,2,2)$ in (5.19):

$$Q_2^{\mathsf{H}}(1 \oplus \tilde{\tilde{o}}_2) Q_2 \mathcal{B}_{2,2}^n Q_2^{\mathsf{H}} (1 \oplus \tilde{\tilde{o}}_2)^{\mathsf{T}} Q_2 = \tilde{\mathcal{B}}_{2,2}^n, \tag{5.21}$$

for $n = 0, 2$. The right-hand side depends affine-linearly on $\tilde{B}_4$ and on no other unknowns. Therefore, we can linearly eliminate $\tilde{B}_4$ from (5.21). We find $5 \times 5 - 9 = 16$ affine-quadratic equations in $\tilde{\tilde{o}}_2$ for $n = 0, 2$. We solve the resulting polynomial system of these 36 equations together with $\tilde{\tilde{o}}_2 \tilde{\tilde{o}}_2^{\mathsf{T}} = \tilde{\tilde{o}}_2^{\mathsf{T}} \tilde{\tilde{o}}_2 = I$ in the variables $\tilde{\tilde{o}}_2 \in \mathbb{C}^{16}$ using the software [12]. Four isolated multiplicity-1 solutions are computed: $\tilde{\tilde{o}}_2^{(1)}, \tilde{\tilde{o}}_2^{(2)}, \tilde{\tilde{o}}_2^{(3)}, \tilde{\tilde{o}}_2^{(4)} \in \mathbb{C}^{16}$. We return to (5.21), substitute in these solutions for $\tilde{\tilde{o}}_2$ and linearly solve for $\tilde{B}_4 \in \mathbb{C}^9$. Corresponding to each $\tilde{\tilde{o}}_2^{(i)}$ we find a unique solution $\tilde{B}_4^{(i)} \in \mathbb{C}^9$. Next up, use (5.19) with $(n,\ell,\ell') = (1,3,1)$:

$$O_3 Q_3 \mathcal{B}_{3,1}^1 = Q_3 \tilde{\mathcal{B}}_{3,1}^1. \tag{5.22}$$

Left-multiplying each side by its transpose yields

$$(\mathcal{B}_{3,1}^1)^{\mathsf{T}} Q_3^{\mathsf{T}} Q_3 \mathcal{B}_{3,1}^1 = (\tilde{\mathcal{B}}_{3,1}^1)^{\mathsf{T}} Q_3^{\mathsf{T}} Q_3 \tilde{\mathcal{B}}_{3,1}^1. \tag{5.23}$$

To evaluate $\tilde{\mathcal{B}}_{3,1}^1$ we plug in the possible values for $\tilde{B}_4$, namely $\tilde{B}_4^{(1)}, \tilde{B}_4^{(2)}, \tilde{B}_4^{(3)}, \tilde{B}_4^{(4)}$, and find that only one of these satisfies (5.23). It is the value that equals B_4, and corresponds to $\tilde{\tilde{o}}_2 = I$ or $\tilde{O}_2 O_2 \tilde{O}_2^{\mathsf{T}} = I$. We conclude $\tilde{B}_4 = B_4$ and $O_2 = I$. Next, we reuse (5.22): since $\tilde{\mathcal{B}}_{3,1}^1 = \mathcal{B}_{3,1}^1$, it says that O_3 fixes a known 7×3 matrix. Similarly to how we utilized (5.20), here we find $\tilde{O}_3 \in O(7,\mathbb{C})$ such that the first three columns of $\tilde{O}_3^{\mathsf{T}}$ span the column space of $Q_1 \tilde{\mathcal{B}}_{3,1}^1$ and $\tilde{O}_3 O_3 \tilde{O}_3^{\mathsf{T}} = I_3 \oplus \tilde{\tilde{o}}_3$ for some $\tilde{\tilde{o}}_3 \in O(4,\mathbb{C})$ where I_3 denotes the 3×3 identity matrix. Then, consider (5.19) with $(n,\ell,\ell') = (1,3,3), (3,3,3)$:

$$Q_3^{\mathsf{H}}(I_3 \oplus \tilde{\tilde{o}}_3) Q_3 \mathcal{B}_{3,3}^n Q_3^{\mathsf{H}} (I_3 \oplus \tilde{\tilde{o}}_3)^{\mathsf{T}} Q_3 = \tilde{\mathcal{B}}_{3,3}^n, \tag{5.24}$$

for $n = 1, 3$. Similarly to how we dealt with (5.21), we linearly eliminate $\tilde{B}_6$ from (5.24). We find $7 \times 7 - 13 = 36$ affine-quadratic equations in $\tilde{\tilde{o}}_3$ for $n = 1, 3$. The polynomial system of these 72 equations with $\tilde{\tilde{o}}_3\tilde{\tilde{o}}_3^\mathsf{T} = \tilde{\tilde{o}}_3^\mathsf{T}\tilde{\tilde{o}}_3 = I$ in variables $\tilde{\tilde{o}}_3 \in \mathbb{C}^{16}$ is solved using [12]. The software computes a unique solution, which is multiplicity-1: $\tilde{\tilde{o}}_3 = I$. Hence $\tilde{O}_3 O_3 \tilde{O}_3^\mathsf{T} = I$, or $O_3 = I$. We return to (5.24) which now reads $\mathcal{B}^n_{3,3} = \tilde{\mathcal{B}}^n_{3,3}$ for $n = 1, 3$. Linearly solving for $\tilde{B}_6$ or using Lemma 5.2, deduce $\tilde{B}_6 = B_6$. This wraps up the base case of (5.18). For reproducibility, Julia and Macaulay2 [20] files, with a random instance of (5.19) carrying out the solution procedure described here, shall be made publicly available at a future date.

Let us now turn to the induction step. Thus assume $L \geq 4$, and that (5.18) has been shown for $L-1$. We wish to show (5.18) for L. By the inductive hypothesis, we know $O_\ell = I$ for $0 \leq \ell \leq L-1$ and $B_p = \tilde{B}_p$ for $p = 0, 2, \ldots, 2(L-1)$. We want $O_L = I$ and $\tilde{B}_{2L} = B_{2L}$. We will rely on two lemmas concerning the dependence of $\mathcal{B}^n_{\ell,\ell'}$ on B_p, Lemmas 5.2 and 5.3.

Consider (5.17) for (n, L, ℓ') satisfying $0 \leq \ell' < L, n \equiv L \equiv \ell' \pmod 2$. For these triples $\mathcal{B}^n_{L,\ell'} = \tilde{\mathcal{B}}^n_{L,\ell'}$, because $(\mathcal{B}^n_{L,\ell'})$ depend only on (B_p) with $p \leq 2L-2$, $(\tilde{\mathcal{B}}^n_{L,\ell'})$ depend only on $(\tilde{B}_p)$ with $p \leq 2L-2$ in the same way, and $B_p = \tilde{B}_p$ for $p \leq 2L-2$. Therefore (5.17) reads

$$\mathcal{B}^n_{L,\ell'} = Q_\ell^\mathsf{H} O_\ell^\mathsf{T} Q_\ell \mathcal{B}^n_{\ell,\ell'},$$

where we used $O_{\ell'} = I$. So left multiplication by $Q_L^\mathsf{H} O_L^\mathsf{T} Q_L$ fixes the concatenation of matrices:

$$\big(\mathcal{B}^n_{L,\ell'} : 0 \leq \ell' < L, n \equiv L \equiv \ell' \pmod 2\big).$$

By Lemma 5.3, the concatenation has full column rank. Thus $Q_L^\mathsf{H} O_L^\mathsf{T} Q_L = I$, or $O_L = I$.

Next, consider (5.17) for (n, L, L) where $0 \leq n \leq L$ and $n \equiv L \pmod 2$. These read:

$$\mathcal{B}^n_{L,L} = \tilde{\mathcal{B}}^n_{L,L},$$

using $O_L = I$. As $B_p = \tilde{B}_p$ for $p \leq 2L-2$, Lemma 5.2 gives $\tilde{B}_{2L} = B_{2L}$. This finishes the induction step for (5.18).

Putting everything together, we conclude that under Assumption 2.3, the moments $m_1[\Phi, \rho_1]$, $m_2[\Phi, \rho_1]$, $m_2[\Phi, \rho_2]$ uniquely identify Φ and $\rho_2^{\downarrow 2L}$, up to rotation and chirality. $\square$

Lemma 5.2. *Let $P \geq 2L$. If the expansion coefficients $(B_p : 2 \leq p \leq 2L-2, p$ is even$)$ are fixed, then the affine-linear map*

$$B_{2L} \mapsto \big(\mathcal{B}^n_{L,L} : 0 \leq n \leq L, n \equiv L \pmod 2\big) \tag{5.25}$$

is injective.

Proof. In fact, we will show that the affine-linear map

$$B_{2L} \mapsto \mathcal{B}^{\underline{n}}_{L,L} \tag{5.26}$$

is injective, where $\underline{n}$ is the element of $\{0, 1\}$ satisfying $\underline{n} \equiv L \pmod 2$. By (2.12), the linear part of (5.26) (i.e., dropping an additive constant depending only B_p with $p \leq 2L-2$) reads:

$$B_{2L} \;\mapsto\; (\mathcal{B}^{\underline{n}}_{L,L})_{m,m'} = (-1)^{m+\underline{n}} \mathcal{N}^{\underline{n}}_L \mathcal{N}^{\underline{n}}_L \frac{\mathcal{C}_{2L}(L, L, m, -m', \underline{n}, -\underline{n})}{4L+1} B_{2L,m'-m}.$$

By Lemmas 5.4 and 5.5, the coefficient of $B_{2L,m'-m}$ is nonzero for all $-L \leq m, m' \leq L$. Clearly, (5.26) is injective and so is (5.25). $\square$

Lemma 5.3. *Let $L \geq 4$. If the expansion coefficients $(B_p : 2 \leq p \leq 2L-2, p$ is even$)$ are Zariski-generic, then the horizontal concatenation of the matrices*

$$\left(\mathcal{B}^{n}_{L,\ell'} : 0 \leq \ell' < L, n \equiv L \equiv \ell' \pmod 2\right) \tag{5.27}$$

has full column rank.

Proof. Since $\left(\mathcal{B}^{n}_{L,\ell'}\right)$ depend polynomially on (B_p) and full column rank of (5.27) is a Zariski-open condition [40], it is enough to exhibit a *single* instance of B_p such that (5.27) has full column rank. Furthermore, in producing such an instance we can temporarily drop the conjugate symmetry condition in (2.9) on (B_p), because this condition defines a dense subset with respect to the complex Zariski topology. Moreover, we can also temporarily drop the normalization condition in (2.9), because $\left(\mathcal{B}^{n}_{L,\ell'}\right)$ depend homogeneously on (B_p).

Now, let us produce a desired instance. If $L = 4$ or $L = 5$, randomly generate (B_p) and verify that (5.27) has rank $2L+1$ (to be fully rigorous, in exact arithmetic in a finite extension of $\mathbb{Q}$ using the formulas for $\mathcal{C}_{\ell''}(\ell, \ell', m, m', n, n')$ and $\mathcal{N}^{n}_{\ell}$ in the proofs of Lemmas 5.4 and 5.5). Meanwhile, for $L \geq 6$ choose (B_p) as follows:

$$B_{p,u} = \begin{cases} \text{nonzero and sufficiently large in magnitude if } (p,u) = (2L-2, 2) \\ \text{nonzero and sufficiently small in magnitude if } (p,u) = (2L-4, -2L+7) \\ 0 \text{ for all other } (p,u). \end{cases}$$

In (5.27), consider the submatrix $[\mathcal{B}^{\underline{n}}_{L,L-2} | \mathcal{B}^{\underline{n}}_{L,L-4}] \in \mathbb{C}^{(2L+1)\times(4L-10)}$ where $\underline{n} \in \{0, 1\}$ such that $\underline{n} \equiv L \pmod 2$. The rows of the submatrix are indexed by $m \in \{-L, -L+1, \ldots, L\}$. The columns of its first and second block are indexed by $m' \in \{-(L-2), -(L-2)+1, \ldots, L-2\}$ and $m' \in \{-(L-4), -(L-4)+1, \ldots, L-4\}$ respectively. With the above choice of (B_p), the block $\mathcal{B}^{\underline{n}}_{L,L-2}$ has support contained in the main diagonal where $m' - m = -(L-2) - (-L) = 2$ and the off-diagonal where $m' - m = -(L-2) - (L-5) = -2L+7$ by (2.12). Moreover, the entries in the main diagonal are nonzero by Lemmas 5.4 and 5.5, and larger in magnitude than the entries in the off-diagonal. Meanwhile, $\mathcal{B}^{\underline{n}}_{L,L-4}$ is supported on its off-diagonal where $m' - m = -(L-4) - (L-3) = -2L+7$, and these entries are nonzero by Lemmas 5.4 and 5.5. It follows that the leftmost $(2L+1) \times (2L+1)$ submatrix of $[\mathcal{B}^{\underline{n}}_{L,L-2} | \mathcal{B}^{\underline{n}}_{L,L-4}]$ is columnwise diagonally dominant, and therefore of full rank. This finishes the case $L \geq 6$. ☐

Lemma 5.4. *Let integers $\ell, \ell', m, m', n, n'$ satisfy $\ell \geq |m|, |n|$ and $\ell' \geq |m'|, |n'|$. Then the constant $\mathcal{C}_{\ell+\ell'}(\ell, \ell', m, m', n, n')$ (2.14) is nonzero.*

Proof. For all septuples of integers satisfying

$$\ell, \ell', \ell'' \geq 0, \quad |\ell - \ell'| \leq \ell'' \leq \ell + \ell', \quad \ell \geq |m|, |n| \quad \text{and} \quad \ell' \geq |m'|, |n'|,$$

by (2.14) $\mathcal{C}_{\ell''}(\ell,\ell',m,m',n,n') = C(\ell,m;\ell',m'|\ell'',m+m')C(\ell,n;\ell',n'|\ell'',n+n')$; by [14]

$$\begin{aligned}
&C(\ell,m;\ell',m'|\ell'',m+m')\\
&=\sqrt{\frac{(2\ell''+1)(\ell+\ell'-\ell'')!(\ell+\ell''-\ell')!(\ell'+\ell''-\ell)!}{(\ell+\ell'+\ell''+1)!}}\\
&\quad\times\sqrt{(\ell-m)!(\ell+m)!(\ell'-m')!(\ell'+m')!(\ell''-m'')!(\ell''+m'')!}\\
&\quad\times\sum_k \frac{(-1)^k}{k!(\ell+\ell'-\ell''-k)!(\ell-m-k)!(\ell'+m'-k)!(\ell''-\ell'+m+k)!(\ell''-\ell-m'+k)!}
\end{aligned}$$

where the summation is over all integers k such that the argument of every factorial is non-negative; and the analogous formula for $C(\ell,n;\ell',n'|\ell'',n+n')$ holds. In the special case $\ell''=\ell+\ell'$, the summations over k collapse to one term where $k=0$. It follows $C(\ell,m;\ell',m'|\ell+\ell',m+m')\neq 0$ and $C(\ell,n;\ell',n'|\ell+\ell',n+n')\neq 0$, hence $\mathcal{C}_{\ell+\ell'}(\ell,\ell',m,m',n,n')\neq 0$. □

Lemma 5.5. *Let integers ℓ and n satisfy $\ell\geq|n|$ and $\ell\equiv n \pmod 2$. Then the constant $\mathcal{N}_\ell^n$* (2.13) *is nonzero.*

Proof. Under the stated conditions on ℓ and n, by (2.13)

$$\mathcal{N}_\ell^n = \sqrt{\frac{2\ell+1}{4\pi}}\sqrt{\frac{(\ell-n)!}{(\ell+n)!}}P_\ell^n(0),$$

where $P_\ell^n(x)$ denotes an associated Legendre polynomial. By [14], for $-1\leq x\leq 1$ it holds

$$P_\ell^n(x) = \frac{(-1)^n}{2^\ell \ell!}(1-x^2)^{n/2}\frac{d^{\ell+n}}{dx^{\ell+n}}(x^2-1)^\ell.$$

The coefficient of $x^{\ell+n}$ in $(x^2-1)^\ell$ is $\binom{\ell}{(\ell+n)/2}(-1)^{(\ell-n)/2}$, therefore $\frac{d^{\ell+n}}{dx^{\ell+n}}(x^2-1)^\ell|_{x=0} = (\ell+n)!\binom{\ell}{(\ell+n)/2}(-1)^{(\ell-n)/2}$. Hence $P_\ell^n(0)=\frac{(-1)^{(\ell+n)/2}}{2^\ell\ell!}(\ell+n)!\binom{\ell}{(\ell+n)/2}$ and

$$\mathcal{N}_\ell^n = \frac{(-1)^{(\ell+n)/2}}{2^\ell}\sqrt{\frac{2\ell+1}{4\pi}}\,\frac{\sqrt{(\ell+n)!(\ell-n)!}}{(\frac{\ell+n}{2})!(\frac{\ell-n}{2})!}. \tag{5.28}$$

In particular, $\mathcal{N}_\ell^n$ is nonzero as claimed. □

A Derivations of moment formulas

The following sections derive the expansion of the rotational distribution in Section 2.2 and the explicit moment expressions in Section 2.3.

A.1 Derivation of basis expansion for in-plane uniform rotational distribution

We assume that the rotational distribution has density $\rho(R)$ with respect to the uniform distribution $\mathrm{d}R$. By the Peter-Weyl theorem [14, Thm. 8.13], any square integrable function $\rho(R)$ can be expanded as

$$\rho(R) = \sum_{p=0}^{P} \sum_{u,v=-p}^{p} B_{p,u,v} U_{uv}^{p}(R),$$

as $P \to \infty$, where $R \in \mathsf{SO}(3)$ and $U_{uv}^{p}(R)$ is the (u,v)-th entry of the Wigner U-matrix $U^{p}(R) \in \mathbb{C}^{(2p+1)\times(2p+1)}$ [14, Eq. 9.41].

We next show how distributions invariant to in-plane rotations can be expressed as in (2.7). According to the definition (2.6), we have

$$\sum_{p=0}^{P} \sum_{u,v=-p}^{p} B_{p,u,v} U_{uv}^{p}(R) = \sum_{p=0}^{P} \sum_{u,v=-p}^{p} B_{p,u,v} U_{uv}^{p}(Rz(\alpha)) = \sum_{p=0}^{P} \sum_{u,v=-p}^{p} B_{p,u,v} \Big(U^{p}(R) U^{p}(z(\alpha)) \Big)_{uv},$$

where we use the homomorphism property of group representations [14, Page 344] for Wigner U-matrices in the last inequality and

$$U^{p}(z(\alpha)) = \operatorname{diag}(e^{-\mathbf{i}p\alpha}, e^{-\mathbf{i}(p-1)\alpha}, \dots, e^{\mathbf{i}p\alpha}).$$

This gives

$$\sum_{p=0}^{P} \sum_{u,v=-p}^{p} B_{p,u,v} U_{uv}^{p}(R) = \sum_{p=0}^{P} \sum_{u,v=-p}^{p} B_{p,u,v} U_{uv}^{p}(R) e^{iv\alpha},$$

which implies $B_{p,u,v} = 0$ for $v \neq 0$. Thus, $\rho(R)$ admits the expansion

$$\rho(R) = \sum_{p=0}^{P} \sum_{u=-p}^{p} B_{p,u,0} U_{u0}^{p}(R).$$

For simplicity, we drop the zero subscript and write

$$\rho(R)\mathrm{d}R = \sum_{p=0}^{P} \sum_{u=-p}^{p} B_{p,u} U_{u0}^{p}(R)\mathrm{d}R, \tag{A.1}$$

where $\mathrm{d}R$ denotes the uniform distribution and $U_{u0}^{p}(R)$ can explicitly be written as in (2.8).

Also, to ensure that the density $\rho(R)$ is a real valued function, we further impose the constraint

$$\sum_{p=0}^{P} \sum_{u=-p}^{p} B_{p,u} U_{u0}^{p}(R) = \sum_{p=0}^{P} \sum_{u=-p}^{p} \overline{B_{p,u} U_{u0}^{p}(R)}.$$

Noting that $\overline{U^p_{u0}(R)} = (-1)^u U^p_{-u,0}(R)$ [10, Page 68], we obtain the symmetry condition

$$\overline{B_{p,u}} = (-1)^u B_{p,-u}. \tag{A.2}$$

Lastly, since the integral of any density function equals one and $U^0_{00}(R) = 1$ for any $R \in \mathsf{SO}(3)$, applying the orthogonality of the matrix elements $\{U^p_{uv}(R) : p \geq 0, -p \leq u, v \leq p\}$ gives

$$B_{0,0} = \int_{\mathsf{SO}(3)} \sum_{p=0}^{P} \sum_{u=-p}^{p} B_{p,u} U^p_{u0}(R) \mathrm{d}R = \int_{\mathsf{SO}(3)} \rho(R) \mathrm{d}R = 1.$$

A.2 Derivation of moment expansions

Using the Fourier slice theorem [29] and the property of Wigner U-matrices [14, Eqn. 9.49], we can write the *Fourier transform* of the projection images in (1.2) in spherical coordinates (r, θ, φ) as

$$\begin{aligned} \widehat{I}_R(r, \varphi) &= (R^\mathsf{T} \cdot \widehat{\Phi})(r, \tfrac{\pi}{2}, \varphi) = \sum_{\ell=0}^{L} \sum_{m=-\ell}^{\ell} A_{\ell m}(r) \sum_{n=-\ell}^{\ell} U^\ell_{mn}(R) Y^n_\ell(\tfrac{\pi}{2}, \varphi) + \widehat{\varepsilon}(r, \varphi) \\ &= \sum_{\ell=0}^{L} \sum_{m=-\ell}^{\ell} \sum_{n=-\ell}^{\ell} A_{\ell m}(r) U^\ell_{mn}(R) e^{\mathrm{i} n \varphi} N^n_\ell + \widehat{\varepsilon}(r, \varphi), \end{aligned} \tag{A.3}$$

where $\widehat{\varepsilon}$ denotes the Fourier transform of the noise term, and in the last equality we use the explicit expressions for spherical harmonics [14, Eqn. 4.36] and define

$$N^n_\ell = \sqrt{\frac{2\ell+1}{4\pi}} \sqrt{\frac{(\ell-n)!}{(\ell+n)!}} P^n_\ell(0),$$

and $P^n_l(x)$ denotes the associated Legendre polynomials. Note that N^n_ℓ is always real-valued and, by the symmetry property of $P^n_l(x)$ [14, Page 53], we have

$$\begin{aligned} N^{-n}_\ell &= \sqrt{\frac{2\ell+1}{4\pi}} \sqrt{\frac{(\ell+n)!}{(\ell-n)!}} P^{-n}_\ell(0) = \sqrt{\frac{2\ell+1}{4\pi}} \sqrt{\frac{(\ell+n)!}{(\ell-n)!}} \cdot (-1)^n \cdot \frac{(\ell-n)!}{(\ell+n)!} P^n_\ell(0) \\ &= (-1)^n N^n_\ell. \end{aligned} \tag{A.4}$$

A.2.1 First-order moment

We first derive the formula for the first-order population moment. Using (A.3) and applying the zero mean property of Gaussian noise, we can rewrite the first-order population moment from (1.4) as

$$\begin{aligned} m_1(r, \varphi) &= \mathbb{E}_{R,\varepsilon}[\widehat{I_R}(r, \varphi)] = \int_{\mathsf{SO}(3)} \widehat{I}_R(r, \varphi) \rho(R) \mathrm{d}R \\ &= \sum_{\ell=0}^{L} \sum_{m=-\ell}^{\ell} \sum_{n=-\ell}^{\ell} A_{\ell m}(r) e^{\mathrm{i} n \varphi} N^n_\ell \sum_{p=0}^{P} \sum_{u=-p}^{p} B_{p,u} \int_{\mathsf{SO}(3)} U^p_{u0}(R) U^\ell_{mn}(R) \mathrm{d}R. \end{aligned} \tag{A.5}$$

Note that Wigner U-matrices satisfy the orthogonality property [14, Eq. 9.32]

$$\int \overline{U^{\ell}_{mn}(R)} U^{p}_{uv}(R) \mathrm{d}R = \frac{1}{2\ell+1} \mathbf{1}_{\ell=p} \mathbf{1}_{u=m} \mathbf{1}_{v=n},$$

and the symmetry property [10, Page 68]

$$\overline{U^{\ell}_{mn}(R)} = (-1)^{m+n} U^{\ell}_{-m,-n}(R),$$

we can simplify (A.5) to

$$m_1(r,\varphi) = \sum_{\ell=0}^{\min\{L,P\}} \sum_{m=-\ell}^{\ell} (-1)^m \frac{1}{2\ell+1} N^0_\ell \cdot A_{\ell m}(r) B_{\ell,-m}, \tag{A.6}$$

where

$$N^0_\ell = \sqrt{\frac{2\ell+1}{4\pi}} P^0_\ell(0)$$

with

$$P^0_\ell(0) = \begin{cases} (-1)^{\ell/2} \cdot \frac{(\ell-1)!!}{\ell!!}, & \text{if } \ell \text{ is even}, \\ 0, & \text{if } \ell \text{ is odd}. \end{cases}$$

The sum in (A.6) ranges over integer indices (ℓ, m) such that

$$0 \le \ell \le \min\{L,P\}, \quad \ell \text{ is even}, \quad -\ell \le m \le \ell,$$

which gives

$$m_1(r,\varphi) = \sum_{\substack{\ell=0,\\ \ell \text{ even}}}^{\min\{L,P\}} \sum_{m=-\ell}^{\ell} (-1)^m \frac{N^0_\ell A_{\ell m}(r)}{2\ell+1} B_{\ell,-m} = \sum_{\substack{\ell=0,\\ \ell \text{ even}}}^{\min\{L,P\}} \sum_{m=-\ell}^{\ell} \frac{N^0_\ell A_{\ell m}(r)}{2\ell+1} \overline{B_{\ell,m}}. \tag{A.7}$$

Thus, we can write the first-order moment in the following matrix form:

$$m_1(r,\varphi) = \sum_{\ell=0}^{\min\{L,P\}} \sum_{m=-\ell}^{\ell} \frac{N^0_\ell \mathbf{1}_{\{\ell \text{ is even}\}}}{2\ell+1} A_{\ell m}(r) \overline{B_{\ell,m}} = \sum_{0 \le \ell \le \min\{L,P\}} A_\ell(r) (\mathfrak{B}_\ell)^{\mathsf{H}}, \tag{A.8}$$

where the terms

$$A_\ell(r) \in \mathbb{C}^{1\times(2\ell+1)} \quad \text{and} \quad \mathfrak{B}_\ell \in \mathbb{C}^{1\times(2\ell+1)}$$

for $0 \le \ell \le \min\{L,P\}$ are defined by

$$(A_\ell(r))_m = A_{\ell m}(r), \tag{A.9}$$

$$\mathcal{N}^0_\ell = N^0_\ell \cdot \mathbf{1}_{\{\ell \equiv 0 \pmod 2\}} \cdot \mathbf{1}_{\{\ell \ge 0\}}, \tag{A.10}$$

$$(\mathfrak{B}_\ell)_m = \frac{\mathcal{N}^0_\ell B_{\ell,m}}{2\ell+1}, \tag{A.11}$$

for $-\ell \le m \le \ell$. Here $A_\ell(r)$ and $\mathcal{N}^0_\ell$ are the same as defined in (2.11) and (2.13), respectively.

A.2.2 Second-order moment

We now derive the formula for the second-order population moment and prove Proposition 2.2. Using (A.3) and noting that the noise term $\widehat{\varepsilon}$ is independent from the signal term, we cam rewrite the second order population moment from (1.4) as

$$\begin{aligned} m_2(r,\varphi,r',\varphi') &= \mathbb{E}_R[\widehat{I_R}(r,\varphi)\overline{\widehat{I_R}(r',\varphi')}] \\ &= \int_{\mathsf{SO}(3)} \Big(\sum_{\ell=0}^{L}\sum_{m=-\ell}^{\ell}\sum_{n=-\ell}^{\ell} A_{\ell m}(r)U^{\ell}_{mn}(R)e^{\mathbf{i}n\varphi}N^{n}_{\ell}\Big)\Big(\sum_{\ell'=0}^{L}\sum_{m'=-\ell'}^{\ell'}\sum_{n'=-\ell'}^{\ell'} \overline{A_{\ell'm'}(r')}\,\overline{U^{\ell'}_{m'n'}(R)}e^{-\mathbf{i}n'\varphi'}N^{n'}_{\ell'}\Big) \\ &\quad \times \Big(\sum_{p=0}^{P}\sum_{u=-p}^{p} B_{p,u}U^{p}_{u0}(R)\Big)\mathrm{d}R. \end{aligned}$$

The product of two Wigner matrix entries can be expressed as a linear combination of Wigner matrix entries [14, Eqn. 9.64],

$$U^{\ell}_{mn}(R)U^{\ell'}_{m'n'}(R) = \sum_{\ell''=|\ell-\ell'|}^{\ell+\ell'} \mathcal{C}_{\ell''}(\ell,\ell',m,m',n,n')U^{\ell''}_{m+m',n+n'}(R), \tag{A.12}$$

where

$$\mathcal{C}_{\ell''}(\ell,\ell',m,m',n,n') = C(\ell,m;\ell',m'|\ell'',m+m')C(\ell,n;\ell',n'|\ell'',n+n'), \tag{A.13}$$

is the product of two Clebsch-Gordan coefficients. This product is nonzero only if (ℓ,ℓ',ℓ'') satisfy the triangle inequalities $|\ell-\ell'| \le \ell'' \le \ell+\ell'$. Note that we also use the fact that the Clebsch-Gordan coefficient $C(\ell,m;\ell',m'|\ell'',m'')$ is nonzero only if $m''=m+m'$ to simplify the formula in (A.12) [11, Eqn 2.41]. Using the identity $\overline{U^{a}_{b,c}(R)} = U^{a}_{-b,-c}(R)$, we obtain

$$\begin{aligned} &\int_{\mathsf{SO}(3)} U^{\ell}_{mn}(R)\overline{U^{\ell'}_{m'n'}(R)}U^{p}_{u0}(R)\mathrm{d}R \\ &= \int_{\mathsf{SO}(3)} (-1)^{m'+n'}U^{\ell}_{mn}(R)U^{\ell'}_{-m',-n'}(R)U^{p}_{u0}(R)\mathrm{d}R \\ &= \int_{\mathsf{SO}(3)} (-1)^{m'+n'}\sum_{\ell''=|\ell-\ell'|}^{\ell+\ell'} \mathcal{C}_{\ell''}(\ell,\ell',m,-m',n,-n')U^{\ell''}_{m-m',n-n'}(R)U^{p}_{u0}(R)\mathrm{d}R \\ &= \int_{\mathsf{SO}(3)} (-1)^{m+n}\sum_{\ell''=|\ell-\ell'|}^{\ell+\ell'} \mathcal{C}_{\ell''}(\ell,\ell',m,-m',n,-n')\overline{U^{\ell''}_{-m+m',-n+n'}(R)}U^{p}_{u0}(R)\mathrm{d}R \\ &= (-1)^{m+n}\sum_{\ell''=|\ell-\ell'|}^{\ell+\ell'} \mathcal{C}_{\ell''}(\ell,\ell',m,-m',n,-n')\frac{1}{2\ell''+1}\mathbf{1}_{\ell''=p}\mathbf{1}_{m'-m=u}\mathbf{1}_{n=n'}. \end{aligned}$$

It follows that

$$
\begin{aligned}
&m_2(r,\varphi,r',\varphi')\\
&=\sum_{\ell=0}^{L}\sum_{\ell'=0}^{L}\sum_{m=-\ell}^{\ell}\sum_{m'=-\ell'}^{\ell'}\sum_{n=-\ell}^{\ell}\sum_{n'=-\ell'}^{\ell'} e^{\mathbf{i}n\varphi}e^{-\mathbf{i}n'\varphi'}N_\ell^n N_{\ell'}^{n'}A_{\ell m}(r)\overline{A_{\ell'm'}(r')}\\
&\times\sum_{p=0}^{P}\sum_{u=-p}^{p}\sum_{\ell''=|\ell-\ell'|}^{\ell+\ell'} B_{p,u}(-1)^{m+n}\frac{\mathcal{C}_{\ell''}(\ell,\ell',m,-m',n,-n')}{2\ell''+1}\mathbf{1}_{p=\ell''}\mathbf{1}_{u=m'-m}\mathbf{1}_{n=n'}.
\end{aligned}
$$

Rearranging the order of summations gives

$$
\begin{aligned}
&m_2(r,\varphi,r',\varphi')\\
&=\sum_{n=-L}^{L}\sum_{n'=-L}^{L}\sum_{\ell=|n|}^{L}\sum_{\ell'=|n'|}^{L}\sum_{m=-\ell}^{\ell}\sum_{m'=-\ell'}^{\ell'} e^{\mathbf{i}n\varphi}e^{-\mathbf{i}n'\varphi'}N_\ell^n N_{\ell'}^{n'}A_{\ell m}(r)\overline{A_{\ell'm'}(r')}\\
&\times\sum_{p=0}^{P}\sum_{u=-p}^{p}\sum_{\ell''=|\ell-\ell'|}^{\ell+\ell'} B_{p,u}(-1)^{m+n}\frac{\mathcal{C}_{\ell''}(\ell,\ell',m,-m',n,-n')}{2\ell''+1}\mathbf{1}_{p=\ell''}\mathbf{1}_{u=m'-m}\mathbf{1}_{n=n'}.
\end{aligned}
$$

This further gives

$$
\begin{aligned}
&m_2(r,\varphi,r',\varphi')\\
&=\sum_{n=-L}^{L}\sum_{\ell=|n|}^{L}\sum_{\ell'=|n|}^{L} e^{\mathbf{i}n(\varphi-\varphi')}N_\ell^n N_{\ell'}^{n}\\
&\times\sum_{m=-\ell}^{\ell}\sum_{m'=-\ell'}^{\ell'}\sum_{p=0}^{P}\sum_{u=-p}^{p}\sum_{\ell''=|\ell-\ell'|}^{\ell+\ell'} A_{\ell m}(r)\overline{A_{\ell'm'}(r')}B_{p,u}(-1)^{m+n}\mathcal{C}_{\ell''}(\ell,\ell',m,-m',n,-n)\frac{\mathbf{1}_{p=\ell''}\mathbf{1}_{u=m'-m}}{2\ell''+1}\\
&=\sum_{n=-L}^{L}\sum_{\ell=|n|}^{L}\sum_{\ell'=|n|}^{L} e^{\mathbf{i}n(\varphi-\varphi')}N_\ell^n N_{\ell'}^{n}\\
&\quad\times\sum_{\ell''=|\ell-\ell'|}^{\min\{\ell+\ell',P\}}\sum_{\substack{-\ell\le m\le\ell\\-\ell'\le m'\le\ell'\\|m'-m|\le\ell''}}(-1)^{m+n}\mathcal{C}_{\ell''}(\ell,\ell',m,-m',n,-n)\frac{A_{\ell m}(r)\overline{A_{\ell'm'}(r')}}{2\ell''+1}B_{\ell'',m'-m}.
\end{aligned}
$$

According to [18, Lemma D.1], we get $N_\ell^n = 0$ for odd $\ell + n$, which further implies

$$\begin{aligned}
&m_2(r,\varphi,r',\varphi') \\
&= \sum_{n=-L}^{L} e^{\mathbf{i}n(\varphi-\varphi')} \sum_{\substack{|n|\le\ell\le L\\ \ell\equiv n \pmod 2}} \sum_{\substack{|n|\le\ell'\le L\\ \ell'\equiv n \pmod 2}} N_\ell^n N_{\ell'}^n \\
&\quad \sum_{\ell''=|\ell-\ell'|}^{\min\{\ell+\ell',P\}} \sum_{\substack{-\ell\le m\le\ell\\ -\ell'\le m'\le\ell'\\ |m'-m|\le\ell''}} (-1)^{m+n}\mathcal{C}_{\ell''}(\ell,\ell',m,-m',n,-n)\frac{A_{\ell m}(r)\overline{A_{\ell'm'}(r')}}{2\ell''+1} B_{\ell'',m'-m}.
\end{aligned} \tag{A.14}$$

As anticipated by the fact that the rotational distribution ρ is in-plane uniform, the second-order moment depends only on $\varphi - \varphi'$ as shown above. Rearranging the sum and using the notation $\mathcal{N}_\ell^n$ as defined in (2.13) gives

$$\begin{aligned}
&m_2(r,\varphi,r',\varphi') \\
&= \sum_{n=-L}^{L} e^{\mathbf{i}n(\varphi-\varphi')} \sum_{\ell=0}^{L}\sum_{\ell'=0}^{L} \mathcal{N}_\ell^n \mathcal{N}_{\ell'}^n \\
&\sum_{\substack{-\ell\le m\le\ell\\ -\ell'\le m'\le\ell'}} \sum_{\ell''=\max\{|m-m'|,|\ell-\ell'|\}}^{\min\{\ell+\ell',P\}} (-1)^{m+n}\frac{\mathcal{C}_{\ell''}(\ell,\ell',m,-m',n,-n)}{2\ell''+1} A_{\ell m}(r) B_{\ell'',m'-m}\overline{A_{\ell'm'}(r')}.
\end{aligned}$$

Thus, we can write the second-order moment more concisely in the following matrix form:

$$m_2(r,\varphi,r',\varphi') = \sum_{n=-L}^{L} e^{\mathbf{i}n(\varphi-\varphi')} \sum_{0\le\ell\le L}\sum_{0\le\ell'\le L} A_\ell(r)\mathcal{B}_{\ell,\ell'}^n (A_{\ell'}(r'))^{\mathsf{H}}, \tag{A.15}$$

where the terms

$$A_\ell(r) \in \mathbb{C}^{1\times(2\ell+1)}, \quad \mathcal{B}_{\ell,\ell'}^n \in \mathbb{C}^{(2\ell+1)\times(2\ell'+1)},$$

for $\ell,\ell' \in \{0,\dots,L\}$, $n \in \{-L,\dots,L\}$ are defined as (2.11) and (2.12).

In addition, we show the Hermitian property of $(\mathcal{B}_{\ell',\ell}^n)_{m',m}$ for potential application in the paper. By the symmetry property of Clebsh-Gordan coefficients [11, Eqn. 2.47],

$$\begin{aligned}
\mathcal{C}_{\ell''}(\ell',\ell,m',-m,n,-n) &= C(\ell',m';\ell,-m|\ell'',-m+m')\cdot C(\ell',n;\ell,-n|\ell'',0) \\
&= C(\ell,-m;\ell',m'|\ell'',-m+m')\cdot C(\ell,-n;\ell',n|\ell'',0) \\
&= C(\ell,m;\ell',-m'|\ell'',m-m')\cdot C(\ell,n;\ell',-n|\ell'',0) \\
&= \mathcal{C}_{\ell''}(\ell,\ell',m,-m',n,-n).
\end{aligned} \tag{A.16}$$

Applying (A.2) and (A.4), we obtain

$$
\begin{aligned}
\overline{(\mathcal{B}^n_{\ell',\ell})_{m',m}} &= \sum_{\ell''=\max\{|m-m'|,|\ell-\ell'|\}}^{\min\{\ell+\ell',P\}} (-1)^{m'+n}\mathcal{N}^n_{\ell'}\mathcal{N}^n_{\ell}\frac{\mathcal{C}_{\ell''}(\ell',\ell,m',-m,n,-n)}{2\ell''+1}\overline{B_{\ell'',m-m'}} \\
&= \sum_{\ell''=\max\{|m-m'|,|\ell-\ell'|\}}^{\min\{\ell+\ell',P\}} (-1)^{m'+n}\mathcal{N}^n_{\ell'}\mathcal{N}^n_{\ell}\frac{\mathcal{C}_{\ell''}(\ell',\ell,m',-m,n,-n)}{2\ell''+1}(-1)^{m-m'}B_{\ell'',-m+m'} \\
&= \sum_{\ell''=\max\{|m-m'|,|\ell-\ell'|\}}^{\min\{\ell+\ell',P\}} (-1)^{m+n}\mathcal{N}^n_{\ell}\mathcal{N}^n_{\ell'}\frac{\mathcal{C}_{\ell''}(\ell,\ell',m,-m',n,-n)}{2\ell''+1}B_{\ell'',-m+m'} \\
&= (\mathcal{B}^n_{\ell,\ell'})_{m,m'}.
\end{aligned}
$$

Hence, we get

$$
\mathcal{B}^n_{\ell,\ell'} = (\mathcal{B}^n_{\ell',\ell})^{\mathsf{H}}.
$$

Also, according to the definition (2.13), we know $\mathcal{N}^n_{\ell}\mathcal{N}^n_{\ell'} = 0$ whenever $\ell \not\equiv \ell' \pmod 2$, which implies for any $-L \le n \le L$,

$$
\mathcal{B}^n_{\ell,\ell'} = 0,
$$

whenever $\ell \not\equiv \ell' \pmod 2$.

The following is also true:

$$
(\mathcal{B}^{-n}_{\ell',\ell})_{-m',-m} = (-1)^{m-m'} \cdot \overline{(\mathcal{B}^n_{\ell',\ell})_{m',m}} = (-1)^{m-m'} \cdot (\mathcal{B}^n_{\ell,\ell'})_{m,m'}.
$$

References

[1] Emmanuel Abbe, Joao M Pereira, and Amit Singer. Estimation in the group action channel. In *2018 IEEE International Symposium on Information Theory (ISIT)*, pages 561–565. IEEE, 2018.

[2] Sriram Aiyer, Philip R Baldwin, Shi Min Tan, Zelin Shan, Juntaek Oh, Atousa Mehrani, Marianne E Bowman, Gordon Louie, Dario Oliveira Passos, Selena Dordević-Marquardt, et al. Overcoming resolution attenuation during tilted cryo-em data collection. *Nature communications*, 15(1):389, 2024.

[3] Xiao-Chen Bai, Greg McMullan, and Sjors HW Scheres. How cryo-EM is revolutionizing structural biology. *Trends in Biochemical Sciences*, 40(1):49–57, 2015.

[4] Afonso S Bandeira, Ben Blum-Smith, Joe Kileel, Jonathan Niles-Weed, Amelia Perry, and Alexander S Wein. Estimation under group actions: recovering orbits from invariants. *Applied and Computational Harmonic Analysis*, 66:236–319, 2023.

[5] Tamir Bendory and Dan Edidin. The sample complexity of sparse multireference alignment and single-particle cryo-electron microscopy. *SIAM Journal on Mathematics of Data Science*, 6(2):254–282, 2024.

[6] Tamir Bendory, Yuehaw Khoo, Joe Kileel, Oscar Mickelin, and Amit Singer. Autocorrelation analysis for cryo-em with sparsity constraints: Improved sample complexity and projection-based algorithms. *Proceedings of the National Academy of Sciences*, 120(18):e2216507120, 2023.

[7] Tejal Bhamre, Teng Zhang, and Amit Singer. Orthogonal matrix retrieval in cryo-electron microscopy. In *2015 IEEE 12th International Symposium on Biomedical Imaging (ISBI)*, pages 1048–1052. IEEE, 2015.

[8] Tejal Bhamre, Teng Zhang, and Amit Singer. Denoising and covariance estimation of single particle cryo-em images. *Journal of structural biology*, 195(1):72–81, 2016.

[9] Tejal Bhamre, Teng Zhang, and Amit Singer. Anisotropic twicing for single particle reconstruction using autocorrelation analysis, 2017.

[10] Lawrence C Biedenharn, James D Louck, and Peter A Carruthers. *Angular momentum in quantum physics: theory and application*. Cambridge University Press, 1984.

[11] Arno Böhm. *Quantum mechanics: foundations and applications*. Springer Science & Business Media, 2013.

[12] Paul Breiding and Sascha Timme. Homotopycontinuation. jl: A package for homotopy continuation in julia. In *Mathematical Software–ICMS 2018: 6th International Conference, South Bend, IN, USA, July 24-27, 2018, Proceedings 6*, pages 458–465. Springer, 2018.

[13] Ewen Callaway. Revolutionary cryo-EM is taking over structural biology. *Nature*, 578(7794):201–202, 2020.

[14] Gregory S. Chirikjian and Alexander B. Kyatkin. *Harmonic Analysis for Engineers and Applied Scientists: Updated and Expanded Edition*. Courier Dover Publications, 2016.

[15] *NIST Digital Library of Mathematical Functions*. http://dlmf.nist.gov/, Release 1.1.5 of 2022-03-15. Frank W. J. Olver, Adri B. Olde Daalhuis, Daniel W. Lozier, Barry I. Schneider, Ronald F. Boisvert, Charles W. Clark, Bruce R. Miller, Bonita V. Saunders, Howard S. Cohl, and Marjorie A. McClain, eds.

[16] Jia Duan, Xin-Heng He, Shu-Jie Li, and H Eric Xu. Cryo-electron microscopy for gpcr research and drug discovery in endocrinology and metabolism. *Nature Reviews Endocrinology*, 20(6):349–365, 2024.

[17] Dan Edidin and Matthew Satriano. Orbit recovery for band-limited functions. *SIAM Journal on Applied Algebra and Geometry*, 8(3):733–755, 2024.

[18] Zhou Fan, Roy R Lederman, Yi Sun, Tianhao Wang, and Sheng Xu. Maximum likelihood for high-noise group orbit estimation and single-particle cryo-em. *The Annals of Statistics*, 52(1):52–77, 2024.

[19] Joachim Frank. *Three-Dimensional Electron Microscopy of Macromolecular Assemblies: Visualization of Biological Molecules in Their Native State*. Oxford University Press, 2006.

[20] Daniel R. Grayson and Michael E. Stillman. Macaulay2, a software system for research in algebraic geometry. Available at `http://www2.macaulay2.com`.

[21] Denis S Grebenkov and B-T Nguyen. Geometrical structure of laplacian eigenfunctions. *siam REVIEW*, 55(4):601–667, 2013.

[22] Jeremy Hoskins, Yuehaw Khoo, Oscar Mickelin, Amit Singer, and Yuguan Wang. Subspace method of moments for ab initio 3-d single-particle cryo-em reconstruction. *arXiv preprint arXiv:2410.06889*, 2024.

[23] Shuai Huang, Mona Zehni, Ivan Dokmanić, and Zhizhen Zhao. Orthogonal matrix retrieval with spatial consensus for 3d unknown view tomography. *SIAM Journal on Imaging Sciences*, 16(3):1398–1439, 2023.

[24] Zvi Kam. The reconstruction of structure from electron micrographs of randomly oriented particles. *Journal of Theoretical Biology*, 82(1):15–39, 1980.

[25] Werner Kühlbrandt. The resolution revolution. *Science*, 343(6178):1443–1444, 2014.

[26] Eitan Levin, Tamir Bendory, Nicolas Boumal, Joe Kileel, and Amit Singer. 3d ab initio modeling in cryo-em by autocorrelation analysis. In *2018 IEEE 15th International Symposium on Biomedical Imaging (ISBI 2018)*, pages 1569–1573. IEEE, 2018.

[27] Bufan Li, Dongjie Zhu, Huigang Shi, and Xinzheng Zhang. Effect of charge on protein preferred orientation at the air–water interface in cryo-electron microscopy. *Journal of Structural Biology*, 213(4):107783, 2021.

[28] Nicholas F Marshall, Oscar Mickelin, Yunpeng Shi, and Amit Singer. Fast principal component analysis for cryo-electron microscopy images. *Biological imaging*, 3:e2, 2023.

[29] Frank Natterer. *The mathematics of computerized tomography*. SIAM, 2001.

[30] Ali Punjani, John L Rubinstein, David J Fleet, and Marcus A Brubaker. cryosparc: algorithms for rapid unsupervised cryo-em structure determination. *Nature methods*, 14(3):290–296, 2017.

[31] Jean-Paul Renaud, Ashwin Chari, Claudio Ciferri, Wen-ti Liu, Hervé-William Rémigy, Holger Stark, and Christian Wiesmann. Cryo-em in drug discovery: achievements, limitations and prospects. *Nature reviews Drug discovery*, 17(7):471–492, 2018.

[32] Sjors HW Scheres. Relion: implementation of a bayesian approach to cryo-em structure determination. *Journal of structural biology*, 180(3):519–530, 2012.

[33] Peter H Schönemann. A generalized solution of the orthogonal procrustes problem. *Psychometrika*, 31(1):1–10, 1966.

[34] Nir Sharon, Joe Kileel, Yuehaw Khoo, Boris Landa, and Amit Singer. Method of moments for 3d single particle ab initio modeling with non-uniform distribution of viewing angles. *Inverse Problems*, 36(4):044003, 2020.

[35] Wei Shi, Yongfei Cai, Haisun Zhu, Hanqin Peng, Jewel Voyer, Sophia Rits-Volloch, Hong Cao, Megan L Mayer, Kangkang Song, Chen Xu, et al. Cryo-em structure of sars-cov-2 postfusion spike in membrane. *Nature*, 619(7969):403–409, 2023.

[36] Yunpeng Shi and Amit Singer. Ab-initio contrast estimation and denoising of cryo-em images. *Computer methods and programs in biomedicine*, 224:107018, 2022.

[37] Fred J Sigworth. A maximum-likelihood approach to single-particle image refinement. *Journal of structural biology*, 122(3):328–339, 1998.

[38] Fred J Sigworth. Principles of cryo-em single-particle image processing. *Journal of Electron Microscopy*, 65(1):57–67, 2015.

[39] Amit Singer. Mathematics for cryo-electron microscopy. In *Proceedings of the International Congress of Mathematicians: Rio de Janeiro 2018*, pages 3995–4014. World Scientific, 2018.

[40] Andrew J Sommese, Charles W Wampler, et al. *The Numerical solution of systems of polynomials arising in engineering and science*. World Scientific, 2005.

[41] Monique S Straub, Oliver F Harder, Nathan J Mowry, Sarah V Barrass, Jakub Hruby, Marcel Drabbels, and Ulrich J Lorenz. Laser Flash Melting Cryo-EM Samples to Overcome Preferred Orientation. *bioRxiv*, pages 2024–11, 2024.

[42] John H Van Drie and Liang Tong. Cryo-em as a powerful tool for drug discovery. *Bioorganic & medicinal chemistry letters*, 30(22):127524, 2020.

[43] Kutti R Vinothkumar and Richard Henderson. Single particle electron cryomicroscopy: trends, issues and future perspective. *Quarterly reviews of biophysics*, 49:e13, 2016.

[44] Daniel Wrapp, Nianshuang Wang, Kizzmekia S Corbett, Jory A Goldsmith, Ching-Lin Hsieh, Olubukola Abiona, Barney S Graham, and Jason S McLellan. Cryo-em structure of the 2019-nCoV spike in the prefusion conformation. *Science*, 367(6483):1260–1263, 2020.

[45] Andy Zhang, Oscar Mickelin, Joe Kileel, Eric J Verbeke, Nicholas F Marshall, Marc Aurèle Gilles, and Amit Singer. Moment-based metrics for molecules computable from cryo-em images. *Biological Imaging*, pages 1–22, 2024.

[46] Zhizhen Zhao, Yoel Shkolnisky, and Amit Singer. Fast steerable principal component analysis. *IEEE transactions on computational imaging*, 2(1):1–12, 2016.